Theranostic Imaging and Radiopharmaceutical Therapy

22

Heying Duan and Andrei Iagaru

22.1 Introduction

The term *theranostic* is a portmanteau of the Greek words *therapo* (therapy) and *gnosis* (knowing) [3]. Opinions differ on the proper spelling: *theragnostic* or *theranostic*. We prefer *thera**g**nostic*, as this reflects its linguistic roots best, but the editors of this volume have opted to drop the "g," and they (for better or for worse) have final say. Both spellings, however, are acknowledged and are widely used. The principle of theranostics is easily explained: *see what you treat, and treat what you see*. In other words, theranostics is predicated on two steps: (1) using a targeting vector labeled with a diagnostic radionuclide to image a biological marker of disease, and (2) using the very same vector labeled with a therapeutic radionuclide to treat the disease that had been visualized.

The first attempts at clinical theranostics were made in the early 1930s using phosphorus-32 (^{32}P) in the context of leukemia and bone tumors [4]. The big breakthrough, however, came in the form of Saul Hertz's revolutionary work using iodine-131 (^{131}I) for Graves' disease and thyroid cancer [5]. His discovery that ^{131}I destroys thyroid cells while sparing other cells of the body is the foundation of radiopharmaceutical therapy (RPT).

Within a theranostic paradigm, imaging is used to assess whether tumor tissue expresses a sufficient amount of a given molecular target relative to healthy tissue for RPT to be effective and safe. This approach also allows for the evaluation of tumor heterogenicity, as more aggressive and advanced cancers typically lose some of their specific tumor markers. In this case, patients may not benefit from RPT. Imaging thus allows for the stratification of responders (who will receive the treatment) and non-responders (who will not). This concept exemplifies personalized precision medicine.

Because molecular changes in the tumor happen before a size difference can be measured on anatomical imaging, molecular imaging can also play a key role in evaluating early response to treatment and in distinguishing true progression from pseudo-progression. The latter is characterized by a size increase on anatomical imaging despite pronounced tumor uptake of the radiopharmaceutical on molecular imaging. Pseudo-progression is believed to be attributed to edema surrounding tumor necrosis, the necrosis itself, or an infiltration of immune cells [6].

The over-arching goal of RPT is the delivery of tumoricidal doses of radiation to cancer cells while minimizing damage of the surrounding healthy tissue. One of the keys to RPT is choosing the right radionuclide, specifically one boasting emissions with high energy but low penetration

H. Duan · A. Iagaru (✉)
Department of Radiology, Division of Nuclear Medicine and Molecular Imaging, Stanford University, Stanford, CA, USA
e-mail: heying@stanford.edu; aiagaru@stanford.edu

L. Bodei et al. (eds.), *Radiopharmaceutical Therapy*, https://doi.org/10.1007/978-3-031-39005-0_22

range. Radionuclides that emit β-particles are well established, but those that emit heavier α-particles have produced very promising results in recent years. Most interestingly, tumor cells that are refractory to β-emitters have been shown to respond to treatment with α-emitters [7]. Dosimetry calculations can be performed to predict the radiation-absorbed doses to the tumor as well as radiosensitive organs such as the kidneys (through which many radiopharmaceuticals are excreted) and thus ensure the delivery of tumoricidal doses with minimal treatment-related side effects. Several new approaches and software tools—such as voxel-based dosimetry—exist to enable the facile and accurate calculation of dosimetric values [8]. In this context, the goal of theranostics is the use of molecular imaging to facilitate pre-treatment dosimetry calculations that in turn allows for personalized doses and a tailored number of cycles based on the characteristics of a patient's tumors.

22.2 Theranostic Pairs

A lock and key can be used to describe the mechanism of theranostic. In this analogy, the target is the cancer cell, but it is *locked* by a molecular marker such as a receptor or enzyme [9]. The *key* (the ligand or vector) targets the *lock* and must fit perfectly in order to bind to the cell. This *key* comes with a *keyring* (a linker) that holds a *keychain* (the radionuclide) (Fig. 22.1). In one scenario, this radioactive *keychain* will enable the imaging of the *lock*, depicting the tumor's specific molecular marker. In another, it will deliver a highly energetic radionuclide that will therapeutically irradiate the tumor cell.

Taken together, the imaging and therapeutic agents we have discussed above constitute a "theranostic pair." The former can be labeled with a radionuclide that emits either γ-rays that allow for scintigraphy/single photon emission computed tomography (SPECT) or positrons

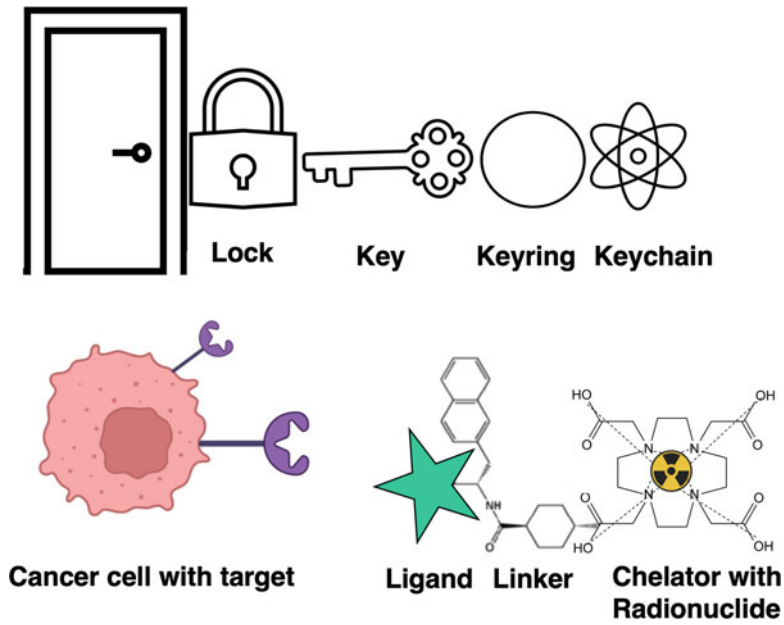

Fig. 22.1 Schematic representation of our *key-lock principle* of theranostics. The target on the cancer cell can be a receptor such as the somatostatin receptor or the human epidermal growth factor receptor-2 (HER-2) or an enzyme such as prostate-specific membrane antigen (PSMA). The matching ligand (or targeting vector) can be a peptide, antibody, or small molecule linked to the chelator, which acts like a cage holding the radionuclide. The radionuclide is chosen according to its application, i.e., ^{99m}Tc, ^{18}F, ^{68}Ga for imaging and ^{177}Lu, ^{90}Y, ^{223}Ra, ^{225}Ac for treatment

that allow for positron emission tomography (PET). Both emissions are characterized by low linear energy transfer (LET), and long radiation range, traits that are ideal for imaging and result in low radiation exposure to the patient. The therapeutic half of this pair, however, is typically labeled with a radionuclide that emits β- or α-particles and exhibits a long half-life (days to weeks), as these traits maximize damage to tumor cells. The emission range of a therapeutic radionuclide reflects its tissue penetration range and determines the size of the area that is irradiated. In some cases, the crossfire effect further enhances treatment to include cells that are not directly targeted but are in the vicinity of those that are.

The ideal theranostic pair employs either a single radionuclide that boasts both therapeutic and "imageable" emissions *or* two radioisotopes of the same element with suitable properties. In this way, the imaging agent and radiotherapeutic are chemically identical, differ only in their isotopic compositions, and thus will exhibit identical in vivo behavior. Along these lines, radioiodine provides an excellent example: ^{123}I and ^{124}I are γ- and positron-emitters, respectively, and are thus suitable for imaging, while ^{131}I is a β-emitter suitable for RPT. Yet isotopologous theranostics are generally the exception, not the rule. To wit, a very commonly used pair of radionuclides in theranostics is gallium-68 (^{68}Ga) for PET and lutetium-177 (^{177}Lu) for treatment. While they are not chemically identical, both can be stably coordinated by the ubiquitous chelator DOTA (as they are in, for example, [^{68}Ga]Ga-DOTA-TATE and [^{177}Lu]Lu-DOTA-TATE). A theranostic pair that is rapidly gaining in interest is copper-64 (^{64}Cu), a positron emitter, and copper-67 (^{67}Cu), a β- and γ-emitter, due to recent advances in the production of ^{67}Cu and highly stable chelators based on sarcophagines, a bicyclic cage-like metal chelator. Table 22.1 gives an overview of radionuclides that may be used in theranostic pairs as well as their physical properties.

RPT is a systemic cytotoxic treatment and is usually administered intravenously (IV) or orally (in the case of ^{131}I), though radioembolization (RE)—a locoregional treatment for primary or secondary liver tumors that is administered directly into the hepatic artery—falls under the RPT umbrella as well. The most widely used radionuclides in RPT are the β-emitters ^{131}I, ^{177}Lu, and yttrium-90 (^{90}Y). The ionizing radiation from these nuclides causes mainly single-strand breaks in DNA, which may lead to the apoptosis of the cancer cell. α-Emitters such as radium-223 (^{223}Ra) and actinium-225 (^{225}Ac) have higher LET and shorter tissue range (<100 μm) and thus cause DNA double-strand breaks with higher frequency, suggesting that they might have even greater antitumoral activity than their β-emitting brethren.

22.3 Thyroid Diseases

The World Health Organization (WHO) recently published the 2022 classification for thyroid neoplasms. Briefly, malignant follicle-derived thyroid neoplasms consist of follicular thyroid carcinoma (FTC), papillary thyroid carcinoma (PTC), invasive encapsulated follicular variant PTC, oncocytic carcinoma, and anaplastic thyroid cancer; medullary thyroid carcinoma (MTC), in contrast, is a C-cell-derived thyroid carcinoma. The vast majority of thyroid cancers are PTC (85%). The incidence of thyroid cancer is now slowly declining after decades of increases that have been retroactively attributed to the evolution of improved diagnostic tools and the overdiagnosis of mostly small and indolent PTCs.

Radioiodide is well suited for theranostics. It boasts both diagnostic and therapeutic radioisotopes and is (of course) structurally identical to iodide, meaning it exhibits the same physiological organification. As a result, radioiodide is taken up and retained in thyroid cells—including well-differentiated thyroid cancer—allowing for both imaging and therapy. The key to this schema is the sodium-iodide symporter (NIS), a transmembrane protein that transports iodide from the bloodstream against a concentration gradient into follicular thyroid cells. Mediated by pendrin channels, this iodide continues to the follicular lumen where thyroid peroxidase organifies the iodide via oxidation to iodine and its subsequent attachment to thyroglobulin.

Table 22.1 Selected clinical theranostic pairs

Disease	Diagnostic	Target	Energy (keV)	Half-life	Therapy	Energy (keV)	Max range	Half-life
DTC Hyperthyroidism	[^{123}I]I$^-$ [^{124}I]I$^-$ [^{99m}Tc]Tc-O_4^-	NIS	159; γ, EC 511; β^+ 140; γ	13.22 h 4.17 d 6.03 h	^{131}I	364; β^-, γ	2.4 mm	8.02 d
Neuroendocrine tumors	[^{68}Ga]Ga-DOTA-TATE [^{68}Ga]Ga-DOTA-TOC [^{68}Ga]Ga-DOTA-NOC [^{64}Cu]Cu-SAR-TATE	SSTR	Mean 890; β^+ 660; β^+, β^-, γ	68 min 12.7 h	[^{177}Lu]Lu-DOTA-TATE [^{90}Y]Y-DOTA-TOC [^{225}Ac]Ac-DOTA-TATE [^{67}Cu]Cu-SAR-TATE	497; β^- 2300; β^- 5800; α 562; β^-	1.7 mm 12 mm <100 μm 2 mm	6.65 d 2.7 d 10 d 2.6 d
Metastatic prostate cancer	[^{68}Ga]Ga-PSMA11 [^{18}F]F-DCFPyL [^{64}Cu]Cu-PSMA [^{68}Ga]Ga-RM2	PSMA GRPR	Mean 890; β^+ 511; β^+ 660; β^+, β^-, γ Mean 890; β^+	68 min 110 min 12.7 h 68 min	[^{177}Lu]Lu-PSMA [^{225}Ac]Ac -PSMA [^{67}Cu]Cu-PSMA [^{177}Lu]Lu-RM2	497; β^- 5800; α 562; β^- 497; β^-	1.7 mm <100 μm 2 mm 1.7 mm	6.65 d 10 d 2.6 d 6.65 d
Bone metastases	[^{99m}Tc]Tc-HDP [^{99m}Tc]Tc-MDP [^{18}F]F-NaF	Bone Hydroxyapatite	140; γ 511; β^+	6.03 h 110 min	[^{223}Ra]$RaCl_2$ [^{153}Sm]Sm-EDTMP	5000–7500; α 640; β^-	<100 μm 3 mm	11.43 d 1.9 d
Neuroblastoma Pheochromocytoma Paraganglioma	[^{123}I]I-mIBG	Norepinephrine transporter	159; γ, EC	13.22 h	[^{131}I]I-mIBG	364; β^-	2 mm	8.02 d
Primary or secondary liver tumors	[^{99m}Tc]Tc-MAA	Direct accumulation	140; γ	6.03 h	[^{90}Y]Y-microspheres	940; β^-	2.4 mm	64.1 h

DTC Differentiated thyroid cancer, *EC* electron capture, *MAA* macroaggregated albumin, *NIS* sodium/iodide symporter

Molecular imaging with a diagnostic isotope of radioiodide can be performed to determine the function of a thyroid nodule (e.g., over-functioning *hot* or non-functioning *cold* nodules [10]) or probe for the presence of hyperthyroidism (Graves' disease, toxic uni- or multinodular adenoma). Imaging with ^{123}I or ^{124}I can be useful for assessing the radioiodine avidity of thyroid lesions, aiding in treatment planning, and avoiding RPT when high activity concentrations are observed in radiosensitive tissues such as the breast or when the thyroid cancer is non-avid for radioiodine.

22.3.1 Differentiated Thyroid Cancer

Therapeutic isotopes of radioiodine—especially ^{131}I—are used for a variety of treatments: to destroy toxic goiter; for whole-organ ablation in Graves' disease; for differentiated thyroid cancer (DTC) after thyroidectomy to ablate any (benign) thyroid remnants so that thyroglobulin decreases to undetectable levels and can be used as tumor marker in follow-up; as adjuvant therapy in DTC to destroy any (unknown) microscopic thyroid cancer cells; and to destroy locoregional or distant metastases in DTC to improve progression-free survival (PFS) and overall survival (OS). A 2019 joint statement from the American Thyroid Association, the European Association of Nuclear Medicine (EANM), the Society of Nuclear Medicine and Molecular Imaging, and the European Thyroid Association (ETA) as well as a recently published 2022 consensus statement of the ETA recommended radioiodine treatment for high-risk and selected cases of intermediate-risk DTC. However, the benefit of radioiodine treatment in low-risk DTC patients is still heavily debated [11, 12]. Importantly, low-risk does not mean no-risk. But how to determine which patient will eventually have recurrent disease? Two large randomized clinical trials are underway to evaluate the benefit of low-dose radioiodine therapy with 1.1 GBq vs. no treatment in patients with low-risk thyroid cancer (NCT01837745, NCT01398085). For high-risk and recurrent disease, a high dose of ≥3.7 GBq ^{131}I is recommended. Post-treatment whole-body scintigraphy (which utilizes the γ-emission of the already administered therapeutic ^{131}I) serves as treatment verification but also shows the true extent of disease and might reveal unsuspected metastases (Fig. 22.2).

Theranostic radioiodine is indispensable for (re-)staging, therapy, and surveillance of DTC. Although DTC has an excellent long-term prognosis—i.e., a five-year survival rate of 97%—recurrence is seen in 5–30% of cases. The treatment of recurrent or metastatic disease becomes problematic when the tumor has lost its functional expression of NIS and is refractory to radioiodine. Unfortunately, efforts to induce redifferentiation with MEK inhibitors such as selumetinib have failed to improve response rate after radioiodine treatment [13].

22.3.2 Medullary Thyroid Cancer

Despite their localization in the thyroid, MTCs are neuroendocrine tumors (NETs) that derive from parafollicular C-cells that arise from the neural crest. After primary treatment surgery, almost 50% of patients show residual or recurrent disease. In advanced, metastatic MTC, treatment options are limited. State-of-the-art multikinase inhibitors have not demonstrated a significant survival benefit but have shown considerable toxicity. As a NET, a fraction of MTC expresses SSTRs that can be targeted by radiolabeled analogs of somatostatin (SSA) for both imaging and treatment. Multiple studies have evaluated peptide receptor radionuclide therapy (PRRT) in MTC and found promising results. Most recently, small studies have shown that [^{177}Lu]Lu-DOTA-TATE produces a high objective response rate (ORR) of 62% and median OS of 26 months [14]. However, PRRT has not yet become clinical routine for MTC given the heterogeneity of the disease and the lack of a unique landmark biological target.

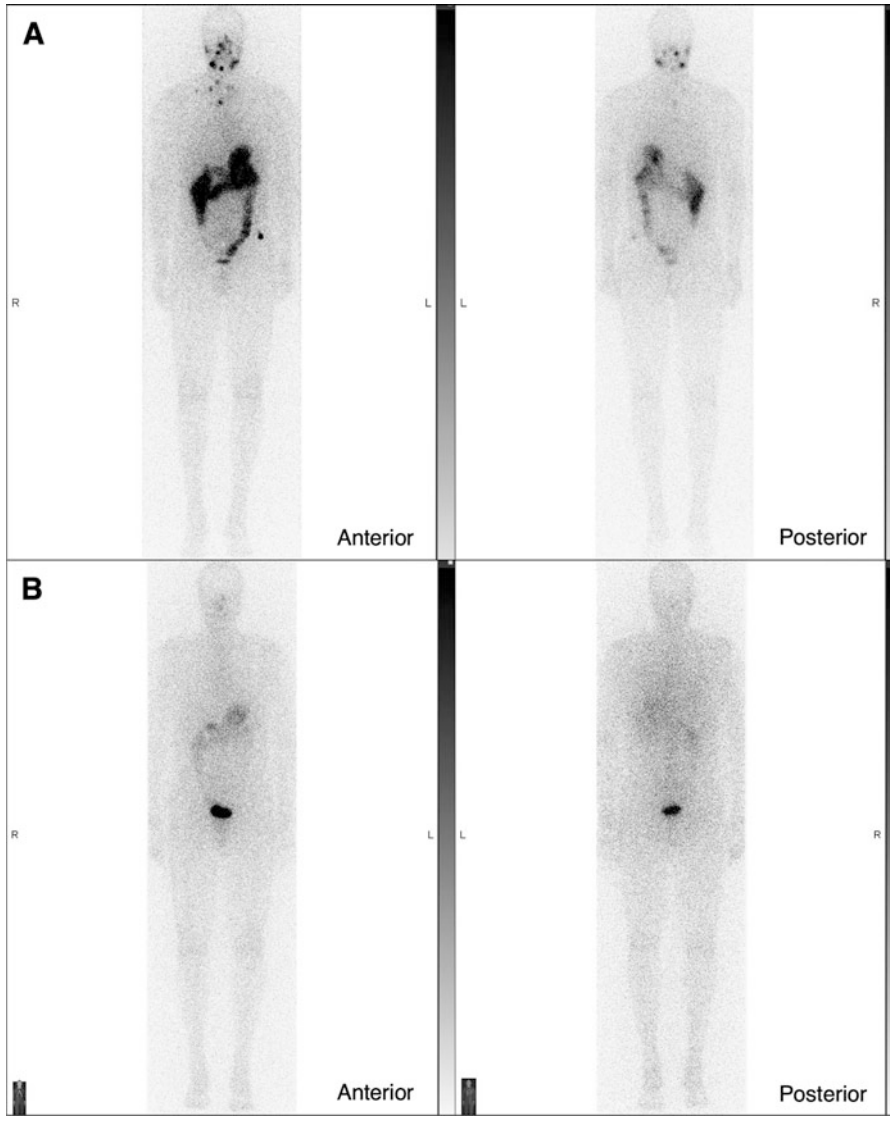

Fig. 22.2 Radioiodine whole-body planar scintigraphy scans of a 34-year-old man with metastatic papillary thyroid cancer. (**a**) After treatment with ^{131}I, multiple foci of uptake in the neck and chest are seen on post-therapeutic imaging. (**b**) In the follow-up diagnostic scintigraphy with ^{123}I, complete response is seen without any pathological uptake

22.4 Neuroendocrine Tumors

NETs derive from neuroendocrine cells and can hence occur in multiple organs, with the majority being gastroenteropancreatic (GEP) and bronchial NETs. These are rare, often slow-growing tumors that are very heterogeneous and only show vague symptoms. Therefore, they are difficult to diagnose, and patients are often misdiagnosed or diagnosed late when the primary tumor has metastasized. Due to the heterogeneity of NETs, their classification and nomenclature is complex. The 2019 WHO classification divides neuroendocrine neoplasia (NEN) into well-differentiated NETs and poorly differentiated

neuroendocrine carcinomas (NECs). NETs can be further stratified by grading based on their mitotic count and Ki-67 index: G1 (Ki67 ≤ 2%), G2 (Ki67 3–20%), and well-differentiated G3 (Ki67 > 20%). NEN can show clinical features that are specific to their organ or cell of origin (e.g., hormone secretion) but can also share characteristics that are independent of the site. Along these lines, all well-differentiated NETs exhibit the overexpression of SSTRs; poorly differentiated NETs and NECs, in contrast, have lesser SSTR expression or have lost it altogether. Five subtypes of human SSTRs have been identified: 1, 2A, 2B, 3, 4, and 5. Most NETs overexpress subtype 2 followed by 5 and 3. The activation of SSTRs results in hormone secretion, thus driving the symptomatic burden of functional NETs. Multiple short- and long-acting SSAs such as octreotide or lanreotide have been developed to target SSTRs and have been shown to relieve NET symptoms and exert an antiproliferative effect [15].

22.4.1 Imaging of NETs

The SPECT imaging of SSTR using [^{111}In]In-octreotide or [^{99m}Tc]Tc-hynic-TOC has been largely replaced by SSTR PET paired with computed tomography (CT) or magnetic resonance imaging (MRI) due to the significantly better image quality and detection rate of the latter (as well as patients' convenience). At present, US Food and Drug Administration (FDA)-approved PET imaging agents based on the DOTA-TOC and DOTA-TATE scaffolds are available. Each has a slightly different affinity to the various SSTR subtypes, but both bind to SSTR2 and have equally high diagnostic accuracies. The US Food and Drug Administration (FDA) has approved [^{68}Ga]Ga-DOTA-TATE, [^{68}Ga]Ga-DOTA-TOC, and [^{64}Cu]Cu-DOTA-TATE for PET imaging. All show high sensitivity, specificity, and accuracy without superiority of one over the other. ^{64}Cu has a longer half-life than ^{68}Ga (12.7 h vs. 68 min), making its central production with long-haul distribution possible. It also allows for delayed imaging with the potential for pre-treatment dosimetry.

22.4.2 Peptide Receptor Radionuclide Therapy

Once NENs have metastasized, treatment options are limited to SSAs, multikinase inhibitors, chemotherapy, locoregional treatments for liver metastases, and, most notably, PRRT (Fig. 22.3). The same SSAs at the heart of the imaging agents described above can be labeled with β-emitters such as ^{177}Lu and ^{90}Y or, more recently, the α-emitter ^{225}Ac for therapy. While the efficacies of [^{90}Y]Y-DOTA-TOC and [^{177}Lu]Lu-DOTA-TATE are similar, [^{90}Y]Y-DOTA-TOC produces increased nephrotoxicity associated with radiation-induced inflammation and fibrosis stemming from its particularly high-energy β-emission.

[^{177}Lu]Lu-DOTA-TATE is now the most widely used tool for the treatment of SSTR-positive NETs. The FDA-approved therapy schema consists of four IV cycles of 7.4 GBq [^{177}Lu]Lu-DOTA-TATE at intervals of 8 weeks. Dose adjustments can be made in the case of bone marrow depression with borderline hematologic parameters such as thrombocytopenia. An amino acid (arginine/lysine) infusion is given immediately before, during, and after the administration of [^{177}Lu]Lu-DOTA-TATE for nephroprotection. Concurrent treatment with long-acting octreotide should be scheduled after PRRT to ensure that the SSTRs are not saturated with the cold analog. Overall, PRRT is a safe treatment with mild side effects [16, 17]. Kidney failure has been reported in the past, but it has not been a significant concern since the introduction of nephroprotection [18].

Even though PRRT has been employed since the early 1990s and there is a large body of literature showing the efficacy of PRRT, most of the studies were from single centers and retrospective. The NETTER-1 trial was the first prospective, randomized, multicenter phase III trial in which patients with midgut NETs were randomized to either receive a high-dose SSA alone (60 mg octreotide LAR) or [^{177}Lu]Lu-DOTA-TATE with best supportive care (30 mg octreotide LAR) [16]. At data-cutoff date, median

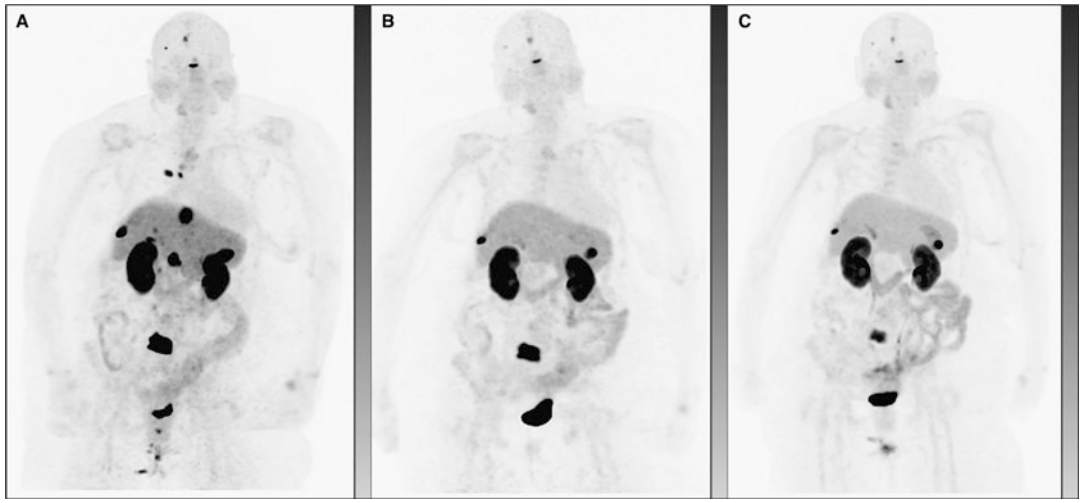

Fig. 22.3 A 69-year-old woman with progressive pancreatic NET, G1. Figures (**a**–**c**) show maximum intensity projections (MIP) of [^{68}Ga]Ga-DOTA-TATE PET: (**a**) pre-treatment evaluation illustrating SSTR overexpression in the primary tumor and metastases; (**b**) interim imaging after two cycles of [^{177}Lu]Lu-DOTA-TATE showing impressive treatment response with markedly decreased tumor burden and resolution of several hepatic and lung lesions; (**c**) imaging after four cycles of PRRT delineating further response in the lumbar vertebra 5 and otherwise stable disease

PFS had not been reached in the PRRT group vs. 8.4 months in the SSA group, which translates to a 79% lower risk of disease progression or death in the PRRT arm. Concordantly, the response rate was significantly higher with [^{177}Lu]Lu-DOTA-TATE (18% vs. 3%). Treatment-related adverse events were higher for PRRT and included nausea and vomiting (attributable to the amino acid infusion), fatigue, abdominal pain, and diarrhea. All were mild and transient. With nephroprotective infusion, grade 3 nephrotoxicity was seen in only 5% (vs. 4% in the control group). Despite similar rates of high-grade adverse events in both groups, neutropenia (1%), thrombocytopenia (2%), and lymphopenia (9%) were unique to PRRT though transient. Patients in the PRRT arm reported a significant improvement in quality of life compared with high-dose SSA. This landmark study led to the 2018 approval of [^{177}Lu]Lu-DOTA-TATE by the FDA and European Medicines Agency for unresectable or metastatic, progressive, well-differentiated, SSTR-positive NETs. The final OS analysis was conducted 5 years after last randomization, with a median observation time of over 6.3 years. Median OS was not statistically significant between both groups: 48.0 months for [^{177}Lu]Lu-DOTA-TATE and 36.3 months for high-dose SSA. However, a high percentage (36%) of patients in the control group crossed over to receive PRRT in follow-up, which may have affected the results for OS. Given that no new long-term toxicity was noted for PRRT with comparable renal toxicity for both groups, the difference of 11.7 months in OS is clinically relevant, therefore favoring PRRT [19].

22.4.3 Theranostics in Advanced Disease

Despite a high Ki-67 index, well-differentiated G3 NETs often still harbor sufficient SSTR for PRRT. Retrospective studies have shown promising results for disease control of up to 72% and PFS of up to 13.1 months [20]. Currently, the NETTER-2 study (NCT03972488) is underway to evaluate the efficacy and safety of [^{177}Lu]Lu-DOTA-TATE as a first-line treatment for well-differentiated but high-grade (Ki67

10–55%) GEP-NETs compared with high-dose octreotide LAR. Other major clinical trials compare PRRT using [^{177}Lu]Lu-edotreotide in high-grade NETs with chemotherapy (NCT04919226) or everolimus (NCT03049189).

The game-changing results with [^{177}Lu]Lu-DOTA-TATE sparked interest in PRRT with α-emitters, particularly in patients who are refractory to [^{177}Lu]Lu-DOTA-TATE despite SSTR-positivity. As the penetration range of α-emitters is short, their toxicity to surrounding healthy tissue is less than that of β-emitters. The first clinical study with [^{225}Ac]Ac-DOTA-TATE was conducted in 32 patients who reached the maximum dosage or failed prior [^{177}Lu]Lu-DOTA-TATE therapy [21]. The interim analysis after a median follow-up of eight months showed a partial response in 63% and stable disease in 37% of the patients who finished two treatment cycles. The toxicity profile was low and similar to [^{177}Lu]Lu-DOTA-TATE: no grade 3 or 4 toxicity was observed. Long-term results of a phase II study with an expanded cohort of 91 patients who received capecitabine as a radiosensitizer prior to [^{225}Ac]Ac-DOTA-TATE with a median follow-up of 24 months showed excellent OS (71%) and PFS (68%) at 24 months as well as response to treatment (3% complete response, 48% partial response, 29% stable disease, 20% progression) [22]. Similar to the pilot study, only minimal toxicities occurred after PRRT. These results warrant future randomized controlled phase III trials comparing [^{225}Ac]Ac-DOTA-TATE and [^{177}Lu]Lu-DOTA-TATE or their sequential administration for the management of NET patients.

22.4.4 Radioembolization of NET Liver Metastases

Up to 91% of GEP-NET patients metastasize to the liver and may develop extensive, bulky disease. As hepatic metastases are the main driver for morbidity and mortality, liver-directed treatment is a local treatment option. Radioembolization with ^{90}Y-microspheres showed a pooled ORR of 51%, estimated disease control of 88%, and median OS of 32 months [23]. In a first-in-human study, [^{213}Bi]Bi-DOTA-TOC was administered intraarterially to patients with progressive, advanced NET liver metastases refractory to [^{177}Lu]Lu-DOTA-TATE and given systemically to one patient with bone marrow carcinosis [24]. The results were very promising, with partial remission or stable disease in all patients. Nephrotoxicity was moderate, and hematotoxicity was less pronounced than with prior β-PRRT, particularly in the patient who was treated systemically. A combination of [^{177}Lu]Lu-DOTA-TATE and RE with ^{166}Ho-micropsheres was also evaluated in a phase II clinical trial with remarkable response in the liver in 43% of patients [25].

22.4.5 SSTR Antagonists

Up until now, only somatostatin agonists have been used for PRRT. Antagonists, however, have been shown to bind to more sites on the SSTR, have a favorable biodistribution, and facilitate better tumor visualization [26]. In a small pilot study, one radiolabeled antagonist—[^{177}Lu]Lu-DOTA-JR11—demonstrated higher tumor radiation doses per administered activity and a seven times higher tumor-to-bone marrow activity concentration ratio compared to [^{177}Lu]Lu-DOTA-TATE [27]. A phase I clinical study evaluated [^{68}Ga]Ga-DOTA-JR11 and [^{177}Lu]Lu-satoreotide tetraxetan ([^{177}Lu]Lu-DOTA-JR11) in patients with advanced SSTR-positive NETs [28]. While the ORR was promising at 45% (including 5% with a complete response), unexpected severe grade 4 hematotoxicity was seen in 4/7 (57%) patients. The reason remains unclear; despite the earliest findings of the pilot study, it cannot be ruled out that the increased binding sites for antagonists, including the bone marrow, result in higher radiation exposure to progenitor cells. A different pair of antagonistic compounds—[^{68}Ga]Ga-NODAGA-LM3 and [^{177}Lu]Lu-DOTA-LM3—have also been evaluated in first-in-human studies [29]. Unlike [^{177}Lu]Lu-DOTA-JR11, only grade 3 thrombocytopenia and lymphopenia were observed in 3/51

(5.9%) and 4/51 (7.8%) patients who were administered [^{68}Ga]Ga-NODAGA-LM3 and [^{177}Lu]Lu-DOTA-LM3, respectively. The mild hematotoxicity might be attributable to the different molecular structure of the two agents or the amount of peptide used in each case.

22.4.6 Other Theranostic Pairs

Another interesting theranostic pair that targets SSTR is [^{64}Cu]/[^{67}Cu]Cu-SAR-TATE. [^{64}Cu]Cu-SAR-TATE PET/CT has demonstrated comparable image quality to [^{68}Ga]Ga-DOTA-TATE 1 h post injection (PI) with high tumor uptake. The lesion-to-liver ratio of [^{64}Cu]Cu-SAR-TATE increased over time, with the highest observed at 24 h PI [30]. The long retention time allows for delayed imaging and therefore pre-treatment dosimetry. ^{67}Cu is a β-emitter with similar LET to ^{177}Lu but has a significantly shorter half-life (2.6 days vs. 6.7 days) that provides a higher dose-rate and potentially greater efficacy. [^{67}Cu]Cu-SAR-TATE recently showed promising tumor growth inhibition in a murine model of SSTR-positive cancer [31]. A phase I/II trial is currently evaluating the dose escalation of [^{67}Cu]Cu-SAR-TATE in pediatric patients with high-risk SSTR-expressing neuroblastoma (NCT04023331).

22.4.7 Treatment Sequence

One particularly important question to address is where to place PRRT in the treatment sequence after progression from first-line treatment with SSAs. The guidelines from the three major NET associations—the European Neuroendocrine Tumor Society, the European Society of Medical Oncology, and the North American Neuroendocrine Tumor Society—are similar and recommend PRRT as the second-line treatment for advanced midgut NETs and the third-line treatment in pancreatic NETs due to a lack of prospective trials. Recently, a multidisciplinary focus group of the EANM reached Delphi consensus on PRRT as the second-line treatment for gastrointestinal (GI) NETs, the first-line treatment for non-resectable or disseminated NET with high SSTR expression, and at first progression in G1-G3 GEP-NETs with sufficient SSTR expression [32].

22.5 Primary and Secondary Liver Tumors

Primary liver tumors include hepatocellular carcinoma (HCC) and intrahepatic cholangiocarcinoma (ICC). Secondary liver malignancies are liver metastases derived from other cancers, most commonly colorectal cancer (CRCLM). The theranostic approach to treat these tumors has many names—selective internal radiation therapy (SIRT), transarterial RE (TARE), or simply RE—but all refer to a technique that is unlike the previously mentioned treatment concepts because it is not given systemically but rather locally, directly at the liver tumors. ^{90}Y-microspheres are administered through a femoral catheter to the tumor-feeding arteries, where the microspheres get trapped as the vessels get smaller and smaller. The tumoricidal effect is induced by internal radiation rather than embolization. The underlying principle is predicated on the dual blood supply to the liver from both the hepatic artery and the portal vein. Liver cells are supplied around 70% by the portal vein and around 30% by the hepatic artery. Liver tumors, however, receive most of their blood from the hepatic artery, which means that a transarterial treatment approach targets liver tumors while sparing normal liver tissue that is mainly provided by the portal system.

Patients with unresectable liver-dominant malignancies with no signs of liver failure (i.e., ascites, elevated total bilirubin level >2 mg/dL), life expectancy of at least 3 months, and Eastern Cooperative Oncology Group Performance Status (ECOG PS) of ≤ 2 with adequate hepatic arterial flow to the cancer(s) can be evaluated for RE. For treatment planning, patients undergo a "mapping" angiography to outline the hepatic arterial flow and identify the tumor-feeding artery/arteries. In some cases, the prophylactic coil embolization of

the extrahepatic vessels arising from the hepatic artery—the right gastric, gastroduodenal, and cystic arteries—might be necessary. This prevents any extrahepatic deposits of microspheres that can cause severe ulcers and inflammation.

22.5.1 Pre-Treatment Planning

[^{99m}Tc]Tc-macroaggregated albumin (MAA) particles are similar in size to the treatment microspheres, and the former are given to provide an estimate of their distribution of the latter. To this end, [^{99m}Tc]Tc-MAA is administered to the vessel(s) that has been selected for treatment. The position of the catheter depends on the area to be treated: proximal to the tumor-feeding artery in case of a single lesion, proximal of the tumor-bearing hepatic lobar artery in case of a radiation segmentectomy/lobectomy, or distal when the whole liver is treated (liver metastases). Post-interventional scintigraphy is performed to estimate the lung shunt fraction (LSF), the fraction of MAA that has escaped the hepatic vascular bed into the pulmonary circulation. SPECT/CT of the liver shows intrahepatic MAA distribution and allows for dosimetry. There are multiple ways to determine the treatment dose, each with certain limitations. The modified body surface area (BSA) method is easy to calculate and commonly used for whole-liver treatment with resin microspheres. It assumes that a larger BSA correlates with a larger liver but does not account for hepatomegaly, prior hepatic resection, obesity, or cachexia. Thus, it tends to underdose large tumors and large livers and overdose small tumors and small livers. The medical internal radiation dose (MIRD) model is based on a single compartment that contains the tumor and the normal liver and assumes the uniform distribution of microspheres within this compartment. In this case, a hypervascular tumor will absorb a higher dose, potentially resulting in over-treatment. Finally, the partition model is the most accurate, as it divides the lung, tumor, and normal liver into separate compartments to estimate their respective radiation absorbed doses but also relies on the concept of a homogenous distribution of particles per compartment. Its limitation is that it can only be used for clearly defined tumors like HCC. Dedicated dosimetry software can aid in dose calculation and personalization to achieve the desired tumor dose while keeping the radiation absorbed dose to healthy liver tissue low.

The treatment procedure is analogous to the planning angiography in which the treatment dose is administered to the tumor-supplying vessel (s) through the same catheter tip position. For ^{90}Y-microspheres, post-treatment imaging with SPECT/CT is challenging, as the emitted bremsstrahlung radiation—i.e., the energy from β-radiation penetrating through tissue—has a broad energy distribution without a well-defined photopeak and is thus difficult to capture. As the decay of ^{90}Y also produces positrons, PET imaging shows higher image quality compared to bremsstrahlung SPECT/CT even at short imaging times [8]. Post-treatment imaging not only enables treatment verification but also helps scout for potential extrahepatic deposits. As collateral vessels form quickly after coil embolization, RE should be performed within 1 week after treatment planning. A schematic representation of the RE workup and workflow shown in Figs. 22.4 and 22.5 shows pre-treatment planning [^{99m}Tc]Tc-MAA SPECT/CT and post-therapeutic ^{90}Y-microsphere PET/CT.

Overall, treatment-related complications and side effects are low [33, 34]. Immediate adverse events include fatigue, nausea, and abdominal pain. Serious complications arise from inadvertent extrahepatic microsphere deposits and are related to their location (i.e., gastritis, duodenitis). Radiation pneumonitis (high LSF) and severe RE-induced liver disease (REILD) are rare but can occur when more than 30 Gy is given to the healthy lung and liver tissue, respectively.

There are two types of ^{90}Y-microspheres with different properties: resin and glass. Glass microspheres are most commonly used for well-defined primary liver cancer, while resin microspheres are mostly used for liver metastases. In addition, holmium-166 (^{166}Ho)

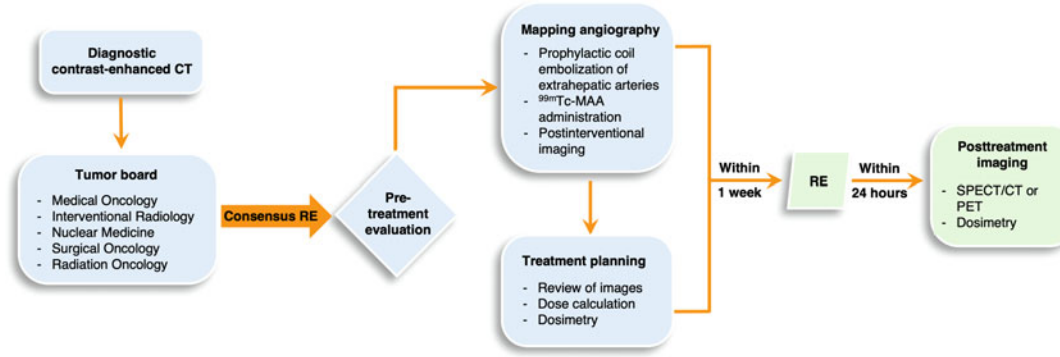

Fig. 22.4 Workup and workflow for radioembolization with ^{90}Y-microspheres

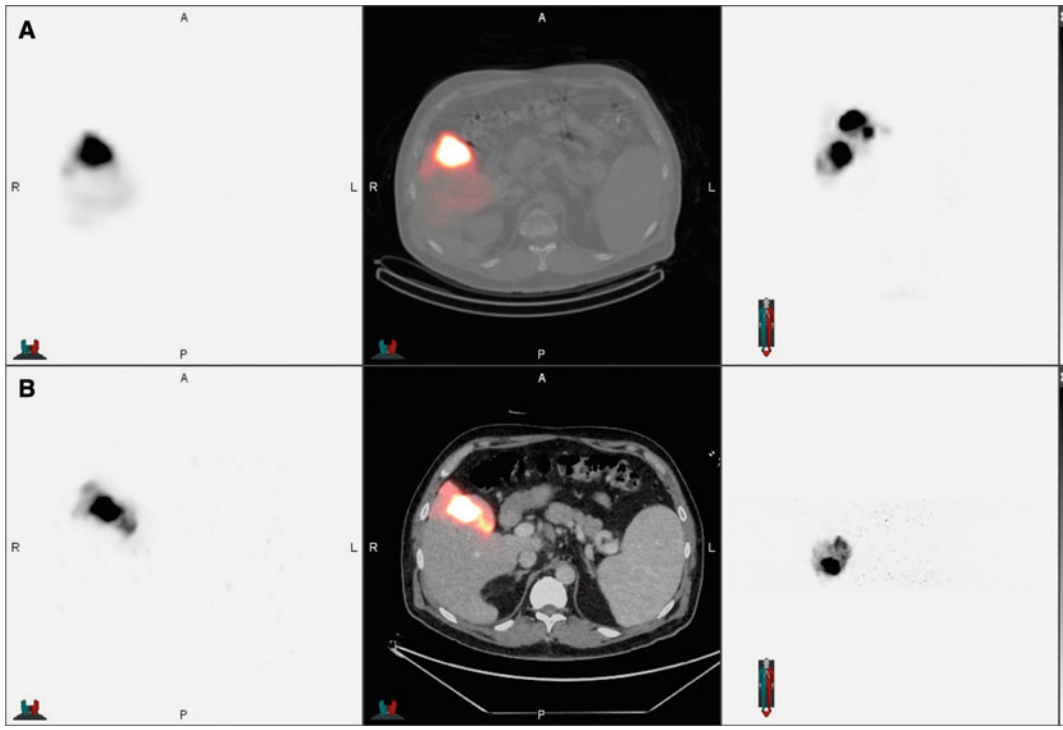

Fig. 22.5 A patient with multifocal HCC presenting for radioembolization of the dominant segment 5 lesion. Pre-treatment planning (**a**) [^{99m}Tc]Tc-MAA SPECT/CT shows MAA distribution in the known tumors in segments 5 and 8 without any extrahepatic deposits. Post-therapeutic (**b**) ^{90}Y-microsphere PET/CT verifies microsphere distribution strictly in the treated segment 5 tumor without any extrahepatic deposits

microspheres are currently under clinical investigation. The benefit in this case is that the β-emitter ^{166}Ho also emits γ-radiation that would allow for therapy planning with the ^{166}Ho-microspheres themselves instead of [^{99m}Tc]Tc-MAA as a surrogate.

22.5.2 Hepatocellular Carcinoma

RE plays a role across all tumor stages of HCC. RE bridges prolonged waiting times to transplantation or downstages to meet Milan criteria for transplantation. This can be achieved by radiation

lobectomy or segmentectomy in which not only the tumor is treated but also hypertrophy of healthy liver is induced. Neoadjuvant RE showed a high ORR of 88% with an OS of 95% and 87% at two years and three years, respectively. Interestingly, survival rates were comparable for patients undergoing subsequent surgery and for those who did not [35]. Long-term follow-up of 15 years in 207 patients who received RE for downstaging or bridging showed a median OS of 12.5 years with a recurrence-free survival of 10 years; only 12% had recurrent disease [36].

In advanced HCC, RE showed a significantly longer time to progression (>26 months) and was better tolerated compared to transarterial chemoembolization (TACE; 6.8 months) [33]. No difference in OS was seen upon comparison to the tyrosine kinase inhibitor sorafenib; however, the reduced toxicity of RE compared to sorafenib affords patients with a higher quality of life and should thus be considered during treatment planning and patient selection [34]. Studies are underway to evaluate the combination of RE and immunotherapy in HCC. RE has been reported to induce the release of tumor-associated antigens that are targeted by antigen-presenting cells. This can lead to a change in the tumor microenvironment (TME) with a potent antitumoral immune response, which could in turn further enhance the efficacy of subsequent immunotherapy. The preliminary results of a trial focused on treatment with nivolumab three weeks after RE revealed favorable tolerability and encouraging response rates [37]. Another randomized trial (NCT04541173) is investigating the safety and effectiveness of RE followed by a combination of atezolizumab and bevacizumab.

22.5.3 Intrahepatic Cholangiocarcinoma

Data on RE in ICC are scarce and involve mostly small cohorts from single centers. A systematic review on RE in treatment-naïve patients showed a prolonged survival, especially when the tumor burden was less than 25% [38]. The combination of chemotherapy and RE led to a longer median OS of up to 24 months compared to chemotherapy and TACE (up to 17 months) [39]. A retrospective study involving 136 patients showed remarkable results: complete response in 2 patients (1.5%), partial response in 42 patients (32.1%), stable disease in 82 patients (62.6%), and progressive disease in only 5 patients (3.8%), with a median OS of 14.2 months [40]. RE was able to downstage 11 patients (8%) to resection, and 2 participants (2%) were bridged to transplant. After resection, the median recurrence and OS were 26.3 and 39.9 months, respectively. Toxicity ≥ grade 3 was seen in 10 patients (8%), and abdominal pain was the leading side effect.

22.5.4 Colorectal Cancer Liver Metastases

Finally, RE was evaluated in patients with unresectable CRCLM in three randomized controlled phase III trials as an addition to first-line treatment with chemotherapy. Even though a delayed progression in the liver was seen, there was no significant OS benefit [41]. However, the major design flaw of this study was that PFS at *any* site was taken as an endpoint for a liver-directed treatment. Current guidelines recommend RE in the salvage setting in which RE has shown a survival benefit.

22.6 Prostate Cancer

Prostate cancer (PC) is the most common cancer in men in the USA, with one in every eight men diagnosed with PC during their lifetime [42]. Despite advances in its management, PC remains the second leading cause of cancer deaths among men. The tumor biology of PC is very heterogeneous and on a spectrum, ranges from indolent disease (Gleason score 3 + 3) to clinically significant, aggressive cancer (Gleason score ≥ 3 + 4), often with reclassification over time. The ease of screening with prostate-specific

antigen (PSA) has led to a dramatic increase in the diagnosis of PC. The over-diagnosis of often insignificant cancers has resulted in over-treatment with its associated risks of erectile dysfunction and incontinence. Given these potentially life-altering side effects, risk stratification is necessary as studies have shown that low-risk disease and some subsets of intermediate-risk indolent disease will benefit from active surveillance, while aggressive cancers merit therapy.

Prostate-specific membrane antigen (PSMA) is a type II transmembrane glycoprotein that is highly overexpressed in over 90% of PCs. A positive correlation between PSMA expression and disease progression has been reported: for example, higher PSMA expression is associated with more advanced, metastasized, and castration-resistant PC (mCRPC). To be fair, the name "PSMA" is a misnomer, as the protein is in fact an enzyme, not an antigen: glutamate carboxypeptidase II. There are many compounds capable of targeting PSMA ranging from peptides and small molecules to antibodies. That said, [^{68}Ga]Ga-PSMA-11 and [^{18}F]F-DCFPyL are the most widely used (and only FDA-approved) radiopharmaceuticals for the imaging of PC. Indeed, the FDA first approved [^{68}Ga]Ga-PSMA-11 in December 2020 for use only at UCLA and UCSF. [^{18}F]F-DCFPyL was approved for US-wide use in May 2021, while [^{68}Ga]Ga-PSMA-11 was approved for widespread use in December of the same year.

Both [^{68}Ga]Ga-PSMA-11 and [^{18}F]F-DCFPyL exhibit high specificity and high tumor uptake and are well suited for patient selection for RPT as they use the same urea-based moiety as a binding motif for PSMA. ^{18}F-labeled DCFPyL has the advantages of higher spatial resolution and better image quality, and its longer half-life (110 min) allows for better tumor-to-background contrast (since the healthy organs have more time for clearance) and facilitates the commercial distribution of the probe. The theranostic pair of [^{64}Cu]Cu- and [^{67}Cu]Cu-SARbisPSMA has also shown promising results in early clinical studies (NCT04868604).

22.6.1 Metastatic Castration-Resistant Prostate Cancer

Once metastatic PC becomes hormone-refractory, treatment options are limited, and the prognosis is poor. PSMA-targeted RPT produced impressive results in the VISION trial, leading to the recent FDA approval of [^{177}Lu]Lu-PSMA-617 for the RPT of mCRPC. An international, multicenter, open-label phase III study enrolled patients with PSMA-positive mCRPC who had previously failed treatment with a next-generation androgen-receptor-pathway inhibitor (i.e., abiraterone, enzalutamide) and taxane-based chemotherapy, and were randomized in a 2:1 ratio to receive either [^{177}Lu]Lu-PSMA-617 plus standard-of-care (SOC) or SOC alone (no other active cytotoxic treatment) [43]. Then, 7.4 GBq [^{177}Lu]Lu-PSMA-617 was administered IV in four cycles with an interval of six weeks. The treatment arm ($n = 551$) showed a significantly longer radiographic PFS (8.7 vs. 3.4 months), OS (15.3 vs. 11.3 months), and time to first symptomatic skeletal event or death (11.5 vs. 6.8 months) than SOC alone ($n = 280$). The response rates to [^{177}Lu]Lu-PSMA-617 were excellent, with 9.2% (vs. 0%) complete response and 41.8% (vs. 3%) partial response along with concordant PSA decreases of up to 80%. Despite a greater incidence of high-grade (≥ grade 3) adverse events related to bone marrow suppression (12.9% anemia, 7.9% thrombocytopenia, and 7.8% lymphopenia), [^{177}Lu]Lu-PSMA-617 was overall well tolerated. Other side effects included fatigue (43.1%), xerostomia (38.8%), and nausea (35.3%), which were all transient. Complementary to the VISION study is TheraP, a randomized multicenter phase II trial in which patients with mCRPC who failed treatment with docetaxel and for whom cabazitaxel was considered the next treatment option were randomized in a 1:1 fashion to receive either [^{177}Lu]Lu-PSMA-617 ($n = 99$) or chemotherapy with cabazitaxel ($n = 101$) [44]. For treatment eligibility, participants underwent both [^{68}Ga]Ga-PSMA-11 and [^{18}F]F-

FDG PET/CT to ensure high PSMA-avidity without any PSMA-negative lesions. A significantly higher decrease in PSA was seen in the [^{177}Lu]Lu-PSMA-617 arm (66%) compared to 37% with cabazitaxel. Concordantly, the ORR was higher for RPT (49% vs. 24%) as well as the 12-month PFS (19% vs. 3%). Interestingly, [^{177}Lu]Lu-PSMA-617 showed fewer adverse events (33% vs. 53%) and more thrombocytopenia (11% vs. 0%), while the cabazitaxel arm exhibited more neutropenia (13% vs. 4%). Among the participants who had pain at baseline, symptomatic relief was higher with RPT vs. chemotherapy (60% vs. 43%). Patient-reported quality of life was similar for both groups at baseline and improved with [^{177}Lu]Lu-PSMA-617, particularly with respect to diarrhea, fatigue, social functioning, and insomnia.

Both the VISION and TheraP trials showed that [^{177}Lu]Lu-PSMA-617 is safe and effective for the RPT of patients with mCRPC who fail androgen-receptor-directed treatment and taxane-based chemotherapy. A larger decrease in PSA was observed in the TheraP trial compared to the VISION trial, a result that could be attributed to the former's strict inclusion criteria of high PSMA-avidity without PSMA-negative lesions. Multiple trials are now underway to evaluate the use of [^{177}Lu]Lu-PSMA-617 earlier in the treatment sequence (NCT04689828 and NCT04720157), even before docetaxel in men with de novo diagnosed metastatic hormone-sensitive PC (NCT04343885), or in combination with immune checkpoint inhibitors (NCT03658447, NCT03805594) and enzalutamide (NCT04419402). Another PSMA-targeting radiotherapeutic—[^{177}Lu]Lu-PSMA I&T—is also under investigation compared to a next-generation androgen-receptor-pathway inhibitor in a phase III trial (NCT04647526).

22.6.2 Alpha Emitters

As in NETs, the RPT of PC using radiotherapeutics labeled with α-emitters is currently of high interest, particularly for patients who are refractory to [^{177}Lu]Lu-PSMA-617. RPT with [^{225}Ac]Ac-PSMA-617 has shown significant decrease in tumor burden and PSA as well as prolonged PFS of 15.2 months and OS of 18 months. Xerostomia was the single most frequent adverse event, occurring after the first treatment cycle. However, despite the concern that the higher LET might lead to higher toxicity, it was not severe enough to discontinue treatment [45]. In a small cohort of patients with advanced mCRPC who failed previous [^{177}Lu]Lu-PSMA-617 therapy, [^{225}Ac]Ac-PSMA-617 produced significant PSA declines with a PFS of 4.1 months and OS of 7.7 months [7]. A tandem technique combining low-dose [^{225}Ac]Ac-PSMA-617 with standard activities of [^{177}Lu]Lu-PSMA-617 reduced the incidence and severity of xerostomia while maintaining the desired antitumor effect [46].

PSMA-targeted RPT with other α-emitters—such as lead-212 (^{212}Pb) and ^{213}Bi—is currently under investigation. [^{213}Bi]Bi-PSMA-617 was explored in a first-in-human study in patients with progressive mCRPC [47]. After two cycles with a cumulative activity of 592 MBq, a radiographic and biochemical response was observed (PSA decline >80%) [47]. Dosimetry, however, renders [^{213}Bi]Bi-PSMA-617 a second choice compared to [^{225}Ac]Ac-PSMA-617 due to the higher perfusion-dependent off-target radiation of [^{213}Bi]Bi-PSMA-617 in the salivary glands and kidneys [48]. In a preclinical study, PSMA-targeting [^{212}Pb]Pb-NG001 produced significant uptake and therapeutic efficacy in mice bearing xenografts of two human PC cell lines with different degrees of PSMA expression: C4-2 (PSMA+) and PC-3 PIP (PSMA+++). Interestingly, the uptake of the radiotherapeutic was only 1.8-fold higher in the PC-3 PIP cells despite their 10-fold higher PSMA expression [49]. Differences in the cellular internalization of natural PSMA-expressing cells compared to the genetically engineered PC-3 PIP cells may explain this discrepancy. Treatment response was better in mice treated with two cycles vs. one cycle. Future clinical studies are warranted.

22.6.3 Gastrin-Releasing Peptide Receptor

Despite its name, PSMA is overexpressed not only by 90% of PCs but also by various other tissues and cancers, leading to false-positive findings. In addition, 10% or greater of PCs are PSMA-negative. As a result, gastrin-releasing peptide receptor (GRPR) has emerged as a promising target alternative to PSMA. GRPR is significantly overexpressed in PC, while the pancreas is the only healthy tissue with high GRPR expression. Initially, agonists were developed to target the receptor, but side effects caused by their internalization prompted a shift toward antagonists. GRPR antagonists have been found to have more binding sites on PC cells, leading to better tumor-to-normal tissue activity concentration ratios.

Many GRPR antagonists have been developed and evaluated preclinically, but only a few have entered the clinic. Among the most studied clinically is RM2. [^{68}Ga]Ga-RM2 shows high tumor uptake and has an overall favorable biodistribution. Compared to PSMA-targeted compounds, the low physiological uptake of GRPR antagonists makes the delineation of pathological abdominal lymph nodes easier. Figure 22.6 shows the biodistribution of [^{68}Ga]Ga-RM2 compared to that of [^{68}Ga]Ga-PSMA-11. [^{68}Ga]Ga-RM2 has demonstrated high detection rates of PC at initial staging [50] as well as at biochemical recurrence [51]. A first-in-human study of ^{177}Lu-labeled RM2 in four patients with mCRPC showed the highest tumor absorbed doses in metastases of bone, lymph nodes, and soft tissue that were all therapeutically relevant [52]. The highest uptake in healthy tissues was seen in the pancreas, making it the dose-limiting organ. However, current thresholds for radiation toxicity to the pancreas are derived from external beam radiation therapy, and it is unknown whether these are transferable to RPT.

In a first-in-man study, another interesting GRPR antagonist—[^{68}Ga]Ga-NeoB (formerly NeoBOMB1)—demonstrated high uptake in pathological PC lesions in primary localized and metastatic PC [53]. [^{68}Ga]Ga-NeoBOMB1 was also explored in GRPR-expressing metastatic GI stromal tumors (GIST) in which high tumor uptake was seen in the majority of patients alongside an excellent safety profile [54]. The theranostic pair of [^{68}Ga]Ga- and [^{177}Lu]Lu-NeoB has shown high GRPR affinity and cell binding as well as high in vivo stability preclinically [53, 55]. A phase I/IIa open-label, multicenter trial is currently underway to evaluate the biodistribution, dosimetry, safety, tolerability, and antitumoral efficacy of [^{177}Lu]Lu-NeoB in patients with GRPR-expressing metastatic solid tumors (NCT03872778). Shifting gears slightly, ^{64}Cu/^{67}Cu-labeled GRPR antagonists conjugated to a novel derivative of sarcophagine—[^{64}Cu]Cu/[^{67}Cu]Cu-SAR-BBN—have shown high affinity for GRPR preclinically [56, 57]. [^{64}Cu]Cu-SAR-BBN is currently being explored in a phase I clinical trial in men with biochemically recurrent PC who are negative on [^{68}Ga]Ga-PSMA-11 PET (NCT05407311).

No correlation has been found between the uptake of PSMA- and GRPR-targeted radiopharmaceuticals, suggesting a complementary relationship between these probes.

Indeed, the molecular interrogation of *both* targets may best reflect the full extent of disease. Along these lines, bispecific compounds that simultaneously target PSMA *and* GRPR have been explored in preclinical studies. The translation of these tools into the clinic is anticipated after they have been shown to be safe and to exhibit suitable radiopharmacokinetics in healthy volunteers [58].

22.7 Bone Metastases

Almost all cancers can spread hematologically to the skeleton, though the most common to follow this pattern include breast, lung, and particularly castration-resistant PC. Bone metastases are frequently categorized as osteoblastic or osteolytic according to their cell of origin. Both interfere with the normal bone cell cycle, leading to either the pronounced breakdown or aberrant

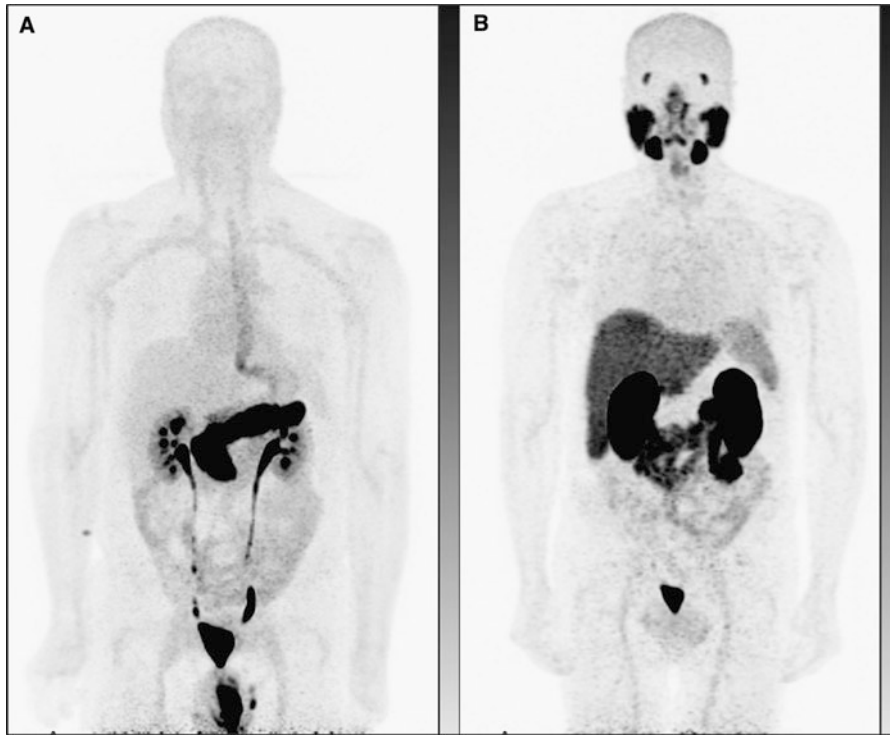

Fig. 22.6 Physiological biodistribution of (**a**) [^{68}Ga]Ga-RM2 and (**b**) [^{68}Ga]Ga-PSMA-11 in a patient with prostate cancer. Most notable is the lower uptake of [^{68}Ga]Ga-RM2 in the gastrointestinal tract. For treatment, the pancreas and the salivary glands are the dose-limiting organs for [^{68}Ga]Ga-RM2 and [^{68}Ga]Ga-PSMA-11, respectively

proliferation of bone tissue. Either process can cause bones to break more easily and can lead to pathologic fractures, pain, hypercalcemia, bone marrow depression, and spinal cord compression. Bone metabolism can be imaged via SPECT with [^{99m}Tc]Tc-bisphosphonates and via PET with sodium fluoride-18 ([^{18}F]F-NaF). Yet since both are bone-seeking agents, only osteoblastic lesions will show uptake. Degenerative skeletal changes are also characterized by enhanced bone activity and can be a differential diagnosis.

Up until the last decade, RPT was only available for bone palliation. Samarium-153 ethylenediamine tetramethylene phosphonate ([^{153}Sm]Sm-EDTMP), a bone-seeking bisphosphonate, produced pain relief within 1–2 weeks along with reduced opioid use and improved quality of life. Despite a delay in skeletal events, however, no significant benefit in OS was seen [59]. As randomized phase III trials were lacking, [^{153}Sm]Sm-EDTMP was not recommended in official guidelines. EDTMP radiolabeled to ^{177}Lu showed promising results for bone palliation in metastatic breast cancer and mCRPC. However, its theranostic partner, [^{68}Ga]-EDTMP, ultimately proved unstable in vivo. The next-generation bisphosphonate zoledronate targets the bone mineral hydroxyapatite and has been radiolabeled with both ^{68}Ga (i.e., [^{68}Ga]Ga-NODAGA^{ZOL}) and ^{177}Lu (i.e., [^{177}Lu]Lu-DOTA-ZOL). In a comparative study of [^{68}Ga]Ga-NODAGA^{ZOL}, [^{68}Ga]Ga-PSMA-11, and [^{99m}Tc]Tc-MDP in patients with advanced PC, [^{68}Ga]Ga-NODAGA^{ZOL} showed better performance in detecting bone lesions at restaging, particularly in patients who failed prior [^{225}Ac]Ac-PSMA-617 treatment. However, [^{68}Ga]Ga-PSMA-11 identified more skeletal metastases at staging at a per-lesion level [60]. [^{68}Ga]Ga-NODAGA^{ZOL}'s therapeutic counterpart, [^{177}Lu]

Lu-DOTA-ZOL, showed high uptake in skeletal metastases and low uptake in the bone marrow in patients with bone metastases secondary to PC [61]. Further prospective studies on the efficacy of treatment with [^{177}Lu]Lu-DOTA-ZOL are warranted.

22.7.1 ^{223}Ra: An Alpha-Emitting Calcium Analog

The α-emitting radiometal ^{223}Ra belongs to the category of calcium analogs that—just like physiological calcium—accumulates in areas of enhanced bone metabolism by forming complexes with the bone mineral hydroxyapatite. The short range of ^{223}Ra's α-particles (< 100 μm) allows for high doses to the osteoblastic tumor while sparing surrounding healthy bone marrow. The safety and efficacy of ^{223}Ra-dichloride ([^{223}Ra]$RaCl_2$) was evaluated in the ALSYMPCA study, a randomized, double-blind, placebo-controlled, multicenter phase III trial [62]. Patients with mCRPC to the bone were randomized to receive [^{223}Ra]$RaCl_2$ or placebo in a 2:1 ratio. The treatment group was administered [^{223}Ra]$RaCl_2$ IV every 4 weeks for up to six cycles, while the placebo group received saline. Patients treated with [^{223}Ra]$RaCl_2$ showed a survival benefit of 3.6 months compared to placebo (14.9 vs. 11.3 months) regardless of prior docetaxel treatment. A delay in time to first symptomatic skeletal event of 5.8 months was seen in the [^{223}Ra]$RaCl_2$ group (15.6 vs. 9.8 months) as well as a 30% reduction in risk of death. Bone pain palliation occurred within two weeks. PSA was unreliable in assessing response to treatment, as only 16% (vs. 6% in the placebo group) of patients showed a decrease in PSA. However, alkaline phosphatase significantly decreased or normalized as sign of therapy response, similar to lactate dehydrogenase. Interestingly, adverse events were less frequent in the [^{223}Ra]$RaCl_2$ group (93% vs. 96%) and included hematotoxicity, particularly anemia and thrombocytopenia, nausea, fatigue, and GI reactions. Predictors for hematotoxicity were prior chemotherapies and extended bone disease. Quality of life improved significantly with [^{223}Ra]$RaCl_2$ and showed a slower decline in the post hoc data analysis. This pivotal study led to the 2013 approval of [^{223}Ra]$RaCl_2$ by the FDA for the RPT of symptomatic bone metastases in patients with mCRPC without known visceral metastases.

Because ^{223}Ra has limited γ-emission, post-treatment imaging is technically possible; however, image quality is poor and scan times are long. The advancement of next-generation SPECT/CT systems based on cadmium zinc telluride (CZT) technology might bring a change (Fig. 22.7). Several studies have investigated the combination of [^{223}Ra]$RaCl_2$ with various other treatment agents. While chemotherapy with docetaxel and paclitaxel paired with [^{223}Ra]$RaCl_2$ has been shown to be safe and produced a longer median time to PSA progression [63, 64], the combination of [^{223}Ra]$RaCl_2$ with abiraterone was unfavorable and led to more fractures and deaths when compared to abiraterone alone [65].

The mode of action of [^{223}Ra]$RaCl_2$ suggests that it may be effective against malignant osteoblastic transformations beyond those caused by mCRPC. The bone metastases in breast cancer, for example, are mostly a mix of osteolytic and osteoblastic lesions. The presence of an osteoblastic portion suggests that ^{223}Ra could be a treatment option. This was investigated in a phase II study for patients with hormone receptor-positive, bone-dominant metastatic breast cancer in which [^{223}Ra]$RaCl_2$ was given concurrently with hormonal therapy [66]. A tumor response rate of 54% and a disease control rate of 49% were seen, leading to a median PFS of 7.4 months and a bone-PFS of 16 months. The treatment was well tolerated, with no grade 3 or 4 adverse events. Studies are now comparing [^{223}Ra]$RaCl_2$ vs. placebo in combination with hormonal therapy and everolimus (NCT02258451) or paclitaxel (NCT04090398).

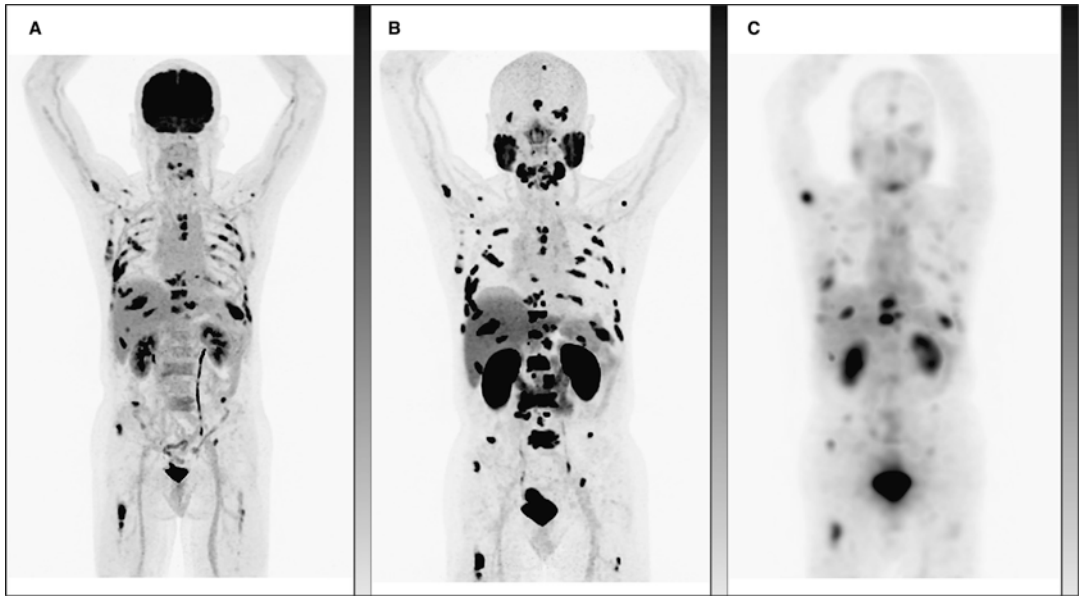

Fig. 22.7 A 66-year-old man with progressive metastatic prostate cancer presenting with PSA 34.7 ng/mL for treatment with [^{177}Lu]Lu-PSMA-617. Pre-treatment [^{18}F]F-FDG PET (MIP, **a**) and [^{18}F]F-DCFPyL PET (MIP, **b**) were performed at 2 min per bed position for a total of 10 min. Both PET scans show an oligometastatic patient with numerous osseous lesions throughout the skeleton. Post-treatment [^{177}Lu]Lu-PSMA-617 SPECT (MIP, **c**) was performed using a next-generation SPECT/CT system based on cadmium zinc telluride technology at 3 min per bed position for four bed positions (12 min total) and shows excellent image quality with high tumor uptake at a significantly reduced acquisition time

22.8 Neuroblastoma, Pheochromocytoma, Paraganglioma

Neuroblastoma, pheochromocytoma, and paraganglioma (PPGL) are orphan diseases (i.e., rare cancers). They are endocrine tumors that arise from neural crest cells, and are characterized by heterogeneous tumor biology. Neuroblastoma is the most common solid childhood tumor and is most commonly found in the adrenal gland. Pheochromocytomas originate from the adrenal medulla, while paragangliomas stem from extra-adrenal, sympathetic (abdomen), or parasympathetic (head and neck) ganglia. Most PPGLs exhibit increased production of catecholamines, leading to hypertension, palpitation, and headache. The tumorigenesis of neuroblastoma and PPGL is characterized by complex molecular pathways with various gene mutations. In unresectable and metastatic cases, treatment options are limited, and the prognosis is poor.

One hallmark of these tumors is the overexpression of the norepinephrine transporter (90% of neuroblastomas, 50–60% of PPGL, and a lower fraction of head and neck paragangliomas). Meta-iodobenzylguanidine (mIBG) is a norepinephrine analog that is actively taken up via norepinephrine transporters, accumulates intracellularly in neuro-secretory granules, and can be radiolabeled with ^{131}I or ^{123}I for theranostic imaging and RPT. [^{131}I]I- or [^{123}I]I-mIBG is typically given first for whole-body imaging to assess the expression of norepinephrine transporters and to determine the extent of disease. Given ^{131}I's long half-life, pre-treatment dosimetry can be performed through serial imaging with [^{131}I]I-mIBG. Subsequent treatment is administered for mIBG-positive tumors for up to two cycles, while post-therapeutic whole-body

scans can be obtained for treatment verification within a week. It is important to note that certain medications (i.e., antihypertensives such as labetalol and calcium channel blockers, antidepressants, tramadol, and pseudoephedrine) should be paused for at least five of their respective half-lives prior to patient evaluation as well as 7 days after diagnostic scans or treatment with [^{131}I]I-mIBG as they interfere with norepinephrine transporters and may cause false-negative scans or a priori transporter saturation. That said, patients should be on an antihypertensive regimen, as worsening hypertension may occur within 24 h of the administration of [^{131}I]I-mIBG. Prophylactic thyroid blockade should also be given at least 24 h prior to treatment and for 10 days afterward, as [^{131}I]I-mIBG usually contains a small quantity of unbound iodine that may be taken up by the thyroid gland otherwise.

In the study that led to the FDA approval of [^{131}I]I-mIBG for PPGL, 68 patients with mIBG-positive, unresectable, or metastatic PPGL with hypertension were treated with one to two cycles of [^{131}I]I-mIBG [67]. Treatment response was seen in 22% of patients after a single cycle and increased to 30% of patients after two cycles. The majority of patients showed stable disease, while 8% progressed. The median OS was 37 months and was longer in patients who received two cycles (44 months vs. 18 months). Symptomatic relief manifested in a ≥50 reduction of all antihypertensive medication for at least 6 months in 25% of patients. A high rate of hematologic adverse events was observed: grade ≥3 hematotoxicity was mostly transient, while 25% required supportive care. Myelodysplastic syndrome was seen in 4% of patients, and secondary leukemias in 3%. A limitation is that patients were not stratified by genetic mutations such as succinate dehydrogenase complex iron sulfur subunit B (SDHB), as the study was designed before their importance was apparent.

Mutations to SDHB are the most common germline mutations in PPGL and a sign of tumor dedifferentiation. Consequently, SDHB mutations are associated with high malignant transformation, metastases, and shorter OS (5-year survival rate 36% vs. 67% in patients without SDHB mutation). The loss of norepinephrine transporter expression is concomitant with tumor dedifferentiation, resulting in false-negative [^{131}I]I-mIBG scans. Furthermore, patients with metastatic, extra-adrenal primaries, and familial PPGL may also exhibit low [^{131}I]I-mIBG avidity. In these patients, SSTR-targeted PRRT might be a viable treatment option (Fig. 22.8).

22.8.1 Peptide Receptor Radionuclide Therapy in Pheochromocytoma and Paraganglioma

Most studies of PRRT in PPGL have been retrospective and comprised of small cohorts. However, an impressive pooled disease control rate of 84% and an ORR of 25% have been reported for PRRT in these patients as well as a more favorable toxicity profile compared to [^{131}I]I-mIBG [68]. Recently, RPT with [^{225}Ac]Ac-DOTATATE was evaluated in patients with metastatic paraganglioma refractory to [^{177}Lu]Lu-DOTATATE and produced a notably high ORR of 50%, a disease control rate of 88%, and a concordant reduction in antihypertensive drugs. The treatment was well tolerated with improvement in ECOG PS [69]. A study combining [^{131}I]I-mIBG and [^{90}Y]Y-DOTA-TOC is now underway (NCT03044977).

22.8.2 Neuroblastoma

For high-risk and relapsed neuroblastoma, a combination of treatments including chemotherapy, radiotherapy, and autologous stem cell transplantation (ASCT) are commonly employed. Monotherapy with [^{131}I]I-mIBG produced a promising 30–40% response rate, so combination therapies with [^{131}I]I-mIBG alongside chemotherapeutic agents such as topotecan, cisplatin, cyclophosphamide, and melphalan have been

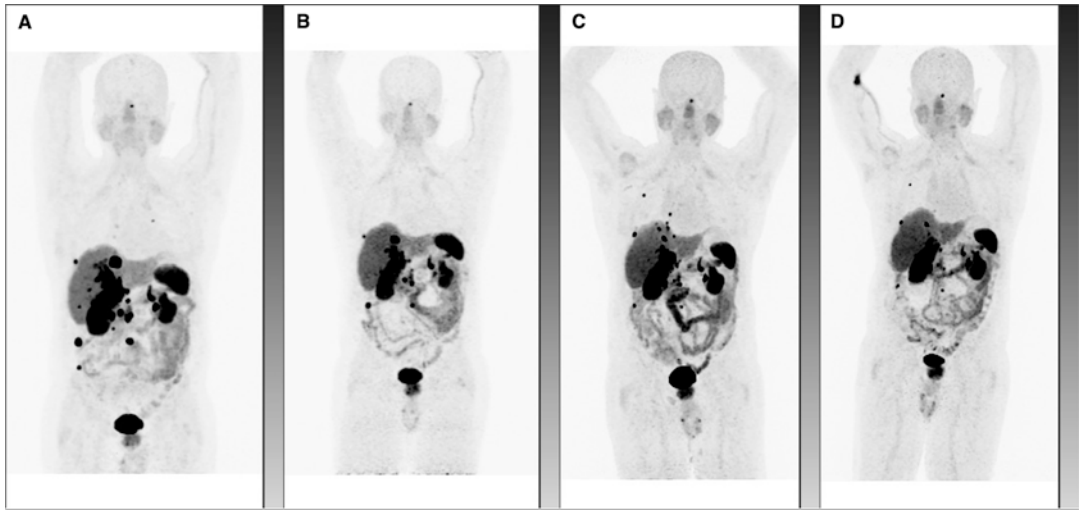

Fig. 22.8 A 73-year-old man with progressive metastatic pheochromocytoma. Figures (**a**–**d**) show maximum intensity projections (MIP) of [^{68}Ga]Ga-DOTA-TATE PET: (**a**) pre-treatment evaluation illustrating SSTR overexpression in all known metastases; (**b**) imaging after four cycles of PRRT with [^{177}Lu]Lu-DOTA-TATE delineating response to treatment with lesional size decreases and the resolution of several hepatic and lung lesions; (**c**) progressive disease with new lesions two years after PRRT; (**d**) after two additional cycles of [^{177}Lu]Lu-DOTA-TATE, favorable treatment response with size decrease in all lesions and the resolution of some hepatic lesions

explored and have yielded response rates ranging from 27 to 80% [70]. [^{131}I]I-mIBG has also produced impressive results in newly diagnosed high-risk neuroblastoma: after two cycles of [^{131}I]I-mIBG combined with topotecan as radiosensitizer followed by standard induction treatment, surgery, and myeloablative therapy with subsequent ASCT, overall ORR was 57%, and the primary tumor showed a response rate of 94% [71]. Hematological adverse effects were most common, often amplified by combined chemotherapy. However, high-risk neuroblastoma patients usually have pre-existing bone marrow disease, which contributes to hematotoxicity.

Patients with neuroblastoma and PPGL should be evaluated for the expression of both norepinephrine transporters and SSTRs. In most cases, a radiopharmaceutical that binds one of these two targets will show a higher degree of uptake and thus should be chosen for subsequent treatment. If both targets are equally overexpressed, the patient's characteristics—most importantly their bone marrow reserve—should drive the selection of the radiotherapeutic RPT.

22.9 Future Developments in Theranostics

By their very nature, theranostics are very specific both to their target and their tumor type. This specificity is advantageous when diagnosing and treating a particular disease, but, in a broader sense, it intrinsically limits RPT to a handful of cancer types. To circumvent this challenge, efforts have been made to identify cancer-specific targets that are expressed across a variety of tumors. One approach aims at the microenvironment of solid tumors, as it contributes to the majority of the tumor mass. The TME consists of a wide variety of cells—ranging from vascular cells to immune cells—but the most abundant are cancer-associated fibroblasts (CAF). These stromal cells overexpress a transmembrane glycoprotein called fibroblast activation protein (FAP) that is associated with tumorigenesis, proliferation, and escape from immunosurveillance. Over 90% of epithelial cancers including colorectal, breast, ovarian, lung, pancreatic, and PC

overexpress FAP. Since its expression in healthy tissue is low, it is suitable as a *broad-spectrum* tumor target.

22.9.1 Fibroblast Activation Protein Inhibitors

FAP inhibitors (FAPI) have been developed for theranostics with promising first clinical results. In a small cohort of patients with sarcoma and pancreatic cancer, [^{90}Y]Y-FAPI-46 showed disease control in 50% of patients as well as a favorable biodistribution profile that could allow for repeat treatment cycles [72]. [^{177}Lu]Lu-FAP-2286 demonstrated high tumor uptake with long retention and reasonable adverse events in patients with metastasized pancreatic, breast, ovarian, and colorectal carcinoma [73]. [^{68}Ga]Ga-FAP-2286 (NCT04621435) and [^{177}Lu]Lu-FAP-2286 (NCT04939610) are currently being evaluated in patients with metastatic FAP-expressing solid tumors to determine their feasibility, efficacy, and safety.

22.9.2 The CXCL12/CXCR-4 Pathway

A distinctive feature of cancer is its ability to evade the immune system. More specifically, it is a disrupted balance of host immunity and tumor growth that leads to tumor progression. In the TME, stromal and immune cells express chemokines that regulate tumor proliferation. The stromal chemokine CXCL12 and its receptor, CXC-chemokine receptor type 4 (CXCR-4), recruit regulatory T-cells that suppress the function of tumor-infiltrating lymphocytes (TILs). TILs, on the other hand, represent host immunity and create a pro-inflammatory environment to kill tumor cells. As cancer is conniving, it upregulates the expression of CXCR-4 on its surface, which in turn stimulates the production of CXCL12 in the TME. The interaction of CXCL12 and CXCR-4 prevents the TILs from deploying their antitumor activity. Thus, the cancer is able to evade the immune system. The activated CXCL12/CXCR4 axis plays a significant role in tumor development and is associated with aggressive tumors [74]. CXCR-4 is particularly overexpressed in cancers of the hematopoietic system. The CXCR-4-targeted theranostic pair of [^{68}Ga]Ga-pentixafor and [^{177}Lu]Lu−/[^{90}Y]Y-pentixather achieved remarkable early results in the clinic: in heavily pre-treated extramedullary relapsed multiple myeloma, an overall ORR of 83% was reported without any acute adverse events [75]. In addition, successful pre-transplant conditioning with desired bone marrow ablation was seen in three patients with refractory acute myeloid leukemia [76]. Finally, in six patients with relapsed diffuse large B-cell lymphoma, CXCR-4 directed RPT in combination with conditioning chemotherapy or radioimmunotherapy led to successful ASCT [77]. Without question, these very promising initial results warrant future studies of CXCR-4-targeted theranostics in solid tumors expressing the receptor.

22.9.3 Pan-Cancer Theranostics

The trend toward a *pan*-cancer theranostic marker may also be achieved with already familiar targets. As mentioned earlier, both PSMA and GRPR are overexpressed in several cancers beyond PC. PSMA-targeted radiopharmaceuticals have been investigated in glioblastoma multiforme, HCC, and renal cell carcinoma, in which uptake has been found in the tumor-associated neovasculature. Furthermore, novel GRPR-antagonists such as NeoBOMB1 and SAR-Bombesin are now being investigated in metastatic gastrointestinal stromal tumors (GIST) and breast cancer (Fig. 22.9), respectively. Early imaging results have been encouraging; however, there is still a long way to go until a therapeutic agent can be translated to the clinic.

Another target of high interest in breast cancer is human epidermal growth factor receptor-2 (HER-2). Variants of the HER-2-targeting antibody trastuzumab have been labeled with various

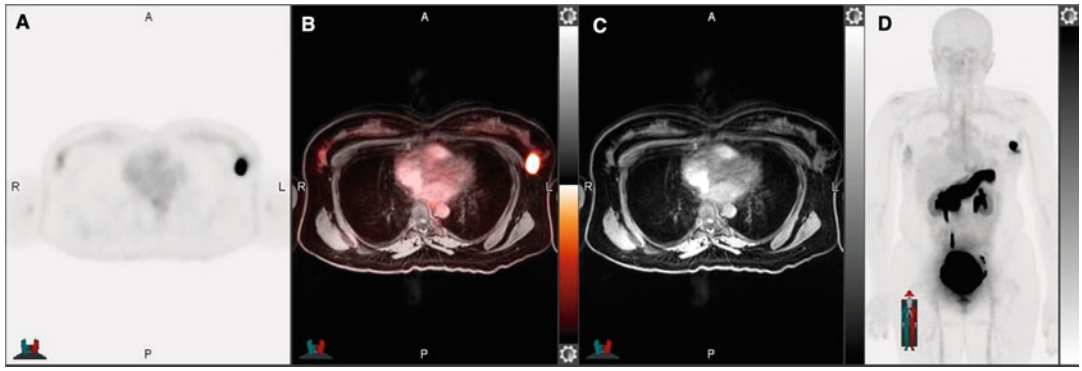

Fig. 22.9 A 36-year-old woman with grade 3 invasive ductal carcinoma. Figures (**a**–**d**) show [^{68}Ga]Ga-RM2 PET/MRI for staging (**a**) axial PET, (**b**) fused axial PET/MRI, (**c**) MRI, and (**d**) maximum intensity projection (MIP) illustrating GRPR overexpression in the left breast mass without evidence for lymph node involvement or distant metastatic disease

positron emitters for imaging such as ^{111}In, ^{124}I, ^{64}Cu, and ^{89}Zr. In a pilot study, a variant of trastuzumab labeled with the therapeutic radionuclide ^{177}Lu has been shown to be well tolerated and has produced high tumor to non-tumor activity concentration ratios as well as satisfactory dosimetry in patients with metastatic HER-2-positive breast cancer [78].

22.9.4 $\alpha_v\beta_6$-Integrin

Another potential target for theranostics is $\alpha_v\beta_6$-integrin, which is overexpressed in epithelial cancers and promotes carcinogenesis. As such, it is found to be markedly overexpressed at the border between tumor and healthy tissue. Many $\alpha_v\beta_6$-targeting compounds have been developed but have also been characterized by high levels of non-specific uptake in the GI system as well as the liver, lungs, and pancreas. A novel, improved compound—[^{68}Ga]Ga-Trivehexin—was recently introduced and has produced promising first results (i.e., high tumor uptake and low non-specific uptake in other organs) in patients with head and neck cancer and pancreatic adenocarcinoma [79].

22.9.5 Moving Forward

In the end, the sheer volume of preclinical studies, clinical studies, and registered new clinical trials on new and established agents bears witness to the high interest and wide range of possibilities of theranostics. Moving forward, future objectives for the field will include the refinement of current therapies with new radiolabeling techniques and chelators to increase the efficacy and safety profile of radiotherapeutics. Furthermore, the best position for many RPTs within the therapeutic sequence needs to be defined, as their value might merit an earlier position in the treatment timeline. Indeed, temporally shifting RPT in this manner may advance it from a palliative to a curative tool. Efforts in dosimetry will allow RPT to move from empiric standardized regimens to personalized treatment doses and cycles. To bring this chapter full circle, we envision that in the future, the language surrounding theranostics in oncology may change from cancer-specific (as in prostate cancer, breast cancer, and neuroendocrine tumors) to molecular phenotype-specific (as in PSMA-expressing, SSTR-expressing, and HER-2-expressing).

22.10 The Bottom Line

- Theranostics is an approach to precision oncology that combines nuclear imaging and radiopharmaceutical therapy using similar targeted radiopharmaceuticals.
- Theranostic radiopharmaceuticals target molecular features on cancer cells for imaging and therapy in an effort to allow clinicians to work according to the maxim "seeing what you treat, and treating what you see."
- Radiotherapeutics produce antitumor activity and symptomatic relief and are ideally characterized by a low-toxicity profile compared to standard chemotherapy, resulting in improved quality of life for patients.
- Prospective clinical trials will pave the way for using RPT earlier in the treatment timeline.

Competing Interests HD and AI declare that they have no conflict of, or competing, interest.

Disclosure Statement The authors have nothing to disclose.

References

1. Bodei L, Herrmann K, Schoder H, Scott AM, Lewis JS. Radiotheranostics in oncology: current challenges and emerging opportunities. Nat Rev Clin Oncol. 2022;19:534–50.
2. Baum RP, Kulkarni HR. THERANOSTICS: from molecular imaging using Ga-68 labeled tracers and PET/CT to personalized radionuclide therapy – the Bad Berka experience. Theranostics. 2012;2:437–47.
3. Frangos S, Buscombe JR. Why should we be concerned about a "g"? Eur J Nucl Med Mol Imaging. 2019;46:519.
4. Erf LA, Lawrence JH. Clinical studies with the aid of radioactive phosphorus. I. The absorption and distribution of radio-phosphorus in the blood and its excretion by normal individuals and patients with leukemia. J Clin Invest. 1941;20:567–75.
5. Hertz S, Roberts A, Salter WT. Radioactive iodine as an indicator in thyroid physiology. Iv. The metabolism of iodine in Graves' disease. J Clin Invest. 1942;21:25–9.
6. Brabander T, van der Zwan WA, Teunissen JJM, et al. Pitfalls in the response evaluation after peptide receptor radionuclide therapy with [(177)Lu-DOTA(0),Tyr(3)]octreotate. Endocr Relat Cancer. 2017;24:243–51.
7. Feuerecker B, Tauber R, Knorr K, et al. Activity and adverse events of Actinium-225-PSMA-617 in advanced metastatic castration-resistant prostate cancer after failure of Lutetium-177-PSMA. Eur Urol. 2021;79:343–50.
8. Duan H, Khalaf MH, Ferri V, et al. High quality imaging and dosimetry for yttrium-90 ((90)Y) liver radioembolization using a SiPM-based PET/CT scanner. Eur J Nucl Med Mol Imaging. 2021;48:2426–36.
9. Jamous M, Haberkorn U, Mier W. Synthesis of peptide radiopharmaceuticals for the therapy and diagnosis of tumor diseases. Molecules. 2013;18:3379–409.
10. Tonacchera M, Viacava P, Agretti P, et al. Benign nonfunctioning thyroid adenomas are characterized by a defective targeting to cell membrane or a reduced expression of the sodium iodide symporter protein. J Clin Endocrinol Metab. 2002;87:352–7.
11. Pacini F, Fuhrer D, Elisei R, et al. ETA Consensus Statement: what are the indications for post-surgical radioiodine therapy in differentiated thyroid cancer? Eur Thyroid J. 2022;2022:11.
12. Tuttle RM, Ahuja S, Avram AM, et al. Controversies, consensus, and collaboration in the use of (131)I therapy in differentiated thyroid cancer: a joint statement from the American Thyroid Association, the European Association of Nuclear Medicine, the Society of Nuclear Medicine and Molecular Imaging, and the European Thyroid Association. Thyroid. 2019;29:461–70.
13. Ho AL, Dedecjus M, Wirth LJ, et al. Selumetinib plus adjuvant radioactive iodine in patients with high-risk differentiated thyroid cancer: a phase III, randomized, placebo-controlled trial (ASTRA). J Clin Oncol. 2022;40:1870–8.
14. Parghane RV, Naik C, Talole S, et al. Clinical utility of (177) Lu-DOTATATE PRRT in somatostatin receptor-positive metastatic medullary carcinoma of thyroid patients with assessment of efficacy, survival analysis, prognostic variables, and toxicity. Head Neck. 2020;42:401–16.
15. Caplin ME, Pavel M, Cwikla JB, et al. Anti-tumour effects of lanreotide for pancreatic and intestinal neuroendocrine tumours: the CLARINET open-label extension study. Endocr Relat Cancer. 2016;23:191–9.
16. Strosberg J, El-Haddad G, Wolin E, et al. Phase 3 trial of (177)Lu-Dotatate for midgut neuroendocrine tumors. N Engl J Med. 2017;376:125–35.
17. Strosberg J, Wolin E, Chasen B, et al. Health-related quality of life in patients with progressive midgut neuroendocrine tumors treated with (177)Lu-Dotatate in the phase III NETTER-1 trial. J Clin Oncol. 2018;36:2578–84.
18. Duan H, Ferri V, Fisher GA, et al. Evaluation of liver and renal toxicity in peptide receptor radionuclide therapy for somatostatin receptor expressing tumors: a 2-year follow-up. Oncologist. 2022;27:447–52.
19. Strosberg JR, Caplin ME, Kunz PL, et al. (177)Lu-Dotatate plus long-acting octreotide versus highdose long-acting octreotide in patients with midgut neuroendocrine tumours (NETTER-1): final overall survival and long-term safety results from an open-label, randomised, controlled, phase 3 trial. Lancet Oncol. 2021;22:1752–63.

20. Raj N, Coffman K, Le T, et al. Treatment response and clinical outcomes of well differentiated high grade neuroendocrine tumors to lutetium-177 DOTATATE. Neuroendocrinology. 2022;112:1177.
21. Ballal S, Yadav MP, Bal C, Sahoo RK, Tripathi M. Broadening horizons with (225)Ac-DOTATATE targeted alpha therapy for gastroenteropancreatic neuroendocrine tumour patients stable or refractory to (177)Lu-DOTATATE PRRT: first clinical experience on the efficacy and safety. Eur J Nucl Med Mol Imaging. 2020;47:934–46.
22. Ballal S, Yadav MP, Tripathi M, Sahoo RK, Bal C. Survival outcomes in metastatic gastroenteropancreatic neuroendocrine tumor patients receiving concomitant (225)Ac-DOTATATE targeted alpha therapy and capecitabine: a real-world scenario management based long-term outcome study. J Nucl Med. 2023;64(2):211–8. https://doi.org/10.2967/jnumed.122.264043
23. Frilling A, Clift AK, Braat A, et al. Radioembolisation with 90Y microspheres for neuroendocrine liver metastases: an institutional case series, systematic review and meta-analysis. HPB (Oxford). 2019;21:773–83.
24. Kratochwil C, Giesel FL, Bruchertseifer F, et al. (2)(1)(3)Bi-DOTATOC receptor-targeted alpha-radionuclide therapy induces remission in neuroendocrine tumours refractory to beta radiation: a first-in-human experience. Eur J Nucl Med Mol Imaging. 2014;41:2106–19.
25. Braat A, Bruijnen RCG, van Rooij R, et al. Additional holmium-166 radioembolisation after lutetium-177-dotatate in patients with neuroendocrine tumour liver metastases (HEPAR PLuS): a single-centre, single-arm, open-label, phase 2 study. Lancet Oncol. 2020;21:561–70.
26. Nicolas GP, Schreiter N, Kaul F, et al. Sensitivity comparison of (68)Ga-OPS202 and (68)Ga-DOTATOC PET/CT in patients with gastroenteropancreatic neuroendocrine tumors: a prospective phase II imaging study. J Nucl Med. 2018;59:915–21.
27. Wild D, Fani M, Fischer R, et al. Comparison of somatostatin receptor agonist and antagonist for peptide receptor radionuclide therapy: a pilot study. J Nucl Med. 2014;55:1248–52.
28. Reidy-Lagunes D, Pandit-Taskar N, O'Donoghue JA, et al. Phase I trial of well-differentiated neuroendocrine tumors (NETs) with radiolabeled somatostatin antagonist (177)Lu-satoreotide tetraxetan. Clin Cancer Res. 2019;25:6939–47.
29. Baum RP, Zhang J, Schuchardt C, Muller D, Macke H. First-in-humans study of the SSTR antagonist (177)Lu-DOTA-LM3 for peptide receptor radionuclide therapy in patients with metastatic neuroendocrine neoplasms: dosimetry, safety, and efficacy. J Nucl Med. 2021;62:1571–81.
30. Hicks RJ, Jackson P, Kong G, et al. (64)Cu-SARTATE PET imaging of patients with neuroendocrine tumors demonstrates high tumor uptake and retention, potentially allowing prospective dosimetry for peptide receptor radionuclide therapy. J Nucl Med. 2019;60:777–85.
31. Cullinane C, Jeffery CM, Roselt PD, et al. Peptide receptor radionuclide therapy with (67)Cu-CuSarTATE is highly efficacious against a somatostatin-positive neuroendocrine tumor model. J Nucl Med. 2020;61:1800–5.
32. Ambrosini V, Kunikowska J, Baudin E, et al. Consensus on molecular imaging and theranostics in neuroendocrine neoplasms. Eur J Cancer. 2021;146:56–73.
33. Salem R, Gordon AC, Mouli S, et al. Y90 radioembolization significantly prolongs time to progression compared with chemoembolization in patients with hepatocellular carcinoma. Gastroenterology. 2016;151:1155–1163 e1152.
34. Venerito M, Pech M, Canbay A, et al. NEMESIS: noninferiority, individual-patient metaanalysis of selective internal radiation therapy with (90)Y resin microspheres versus sorafenib in advanced hepatocellular carcinoma. J Nucl Med. 2020;61:1736–42.
35. Salem R, Johnson GE, Kim E, et al. Yttrium-90 radioembolization for the treatment of solitary, unresectable HCC: the LEGACY study. Hepatology. 2021;74:2342–52.
36. Gabr A, Kulik L, Mouli S, et al. Liver transplantation following Yttrium-90 radioembolization: 15-year experience in 207-patient cohort. Hepatology. 2021;73:998–1010.
37. Chew V, Lee YH, Pan L, et al. Immune activation underlies a sustained clinical response to Yttrium-90 radioembolisation in hepatocellular carcinoma. Gut. 2019;68:335–46.
38. Reimer P, Virarkar MK, Binnenhei M, Justinger M, Schon MR, Tatsch K. Prognostic factors in overall survival of patients with unresectable intrahepatic cholangiocarcinoma treated by means of Yttrium-90 radioembolization: results in therapy-naive patients. Cardiovasc Intervent Radiol. 2018;41:744–52.
39. Cucchetti A, Cappelli A, Mosconi C, et al. Improving patient selection for selective internal radiation therapy of intra-hepatic cholangiocarcinoma: a meta-regression study. Liver Int. 2017;37:1056–64.
40. Gupta AN, Gordon AC, Gabr A, et al. Yttrium-90 radioembolization of unresectable intrahepatic cholangiocarcinoma: long-term follow-up for a 136-patient cohort. Cardiovasc Intervent Radiol. 2022;45(8):1117–28. https://doi.org/10.1007/s00270-022-03183-2
41. Wasan HS, Gibbs P, Sharma NK, et al. First-line selective internal radiotherapy plus chemotherapy versus chemotherapy alone in patients with liver metastases from colorectal cancer (FOXFIRE, SIRFLOX, and FOXFIRE-Global): a combined analysis of three multicentre, randomised, phase 3 trials. Lancet Oncol. 2017;18:1159–71.
42. Siegel RL, Miller KD, Fuchs HE, Jemal A. Cancer statistics, 2022. CA Cancer J Clin. 2022;72:7–33.

43. Sartor O, de Bono J, Chi KN, et al. Lutetium-177-PSMA-617 for metastatic castration-resistant prostate cancer. N Engl J Med. 2021;385:1091–103.
44. Hofman MS, Emmett L, Sandhu S, et al. [(177)Lu]Lu-PSMA-617 versus cabazitaxel in patients with metastatic castration-resistant prostate cancer (TheraP): a randomised, open-label, phase 2 trial. Lancet. 2021;397:797–804.
45. Sathekge M, Bruchertseifer F, Vorster M, et al. Predictors of overall and disease-free survival in metastatic castration-resistant prostate cancer patients receiving (225)Ac-PSMA-617 radioligand therapy. J Nucl Med. 2020;61:62–9.
46. Khreish F, Ebert N, Ries M, et al. (225)Ac-PSMA-617/(177)Lu-PSMA-617 tandem therapy of metastatic castration-resistant prostate cancer: pilot experience. Eur J Nucl Med Mol Imaging. 2020;47:721–8.
47. Sathekge M, Knoesen O, Meckel M, Modiselle M, Vorster M, Marx S. (213)Bi-PSMA-617 targeted alpha-radionuclide therapy in metastatic castration-resistant prostate cancer. Eur J Nucl Med Mol Imaging. 2017;44:1099–100.
48. Kratochwil C, Schmidt K, Afshar-Oromieh A, et al. Targeted alpha therapy of mCRPC: dosimetry estimate of (213)Bismuth-PSMA-617. Eur J Nucl Med Mol Imaging. 2018;45:31–7.
49. Stenberg VY, Tornes AJK, Nilsen HR, et al. Factors influencing the therapeutic efficacy of the PSMA targeting radioligand (212)Pb-NG001. Cancers (Basel). 2022;14(11):2784. https://doi.org/10.3390/cancers14112784
50. Duan H, Baratto L, Fan RE, et al. Correlation of (68)Ga-RM2 PET with postsurgery histopathology findings in patients with newly diagnosed intermediate- or high-risk prostate cancer. J Nucl Med. 2022;63:1829–35.
51. Baratto L, Song H, Duan H, et al. PSMA- and GRPR-targeted PET: results from 50 patients with biochemically recurrent prostate cancer. J Nucl Med. 2021;62:1545–9.
52. Kurth J, Krause BJ, Schwarzenbock SM, Bergner C, Hakenberg OW, Heuschkel M. First-in-human dosimetry of gastrin-releasing peptide receptor antagonist [(177)Lu]Lu-RM2: a radiopharmaceutical for the treatment of metastatic castration-resistant prostate cancer. Eur J Nucl Med Mol Imaging. 2020;47:123–35.
53. Nock BA, Kaloudi A, Lymperis E, et al. Theranostic perspectives in prostate cancer with the gastrin-releasing peptide receptor antagonist NeoBOMB1: preclinical and first clinical results. J Nucl Med. 2017;58:75–80.
54. Gruber L, Jimenez-Franco LD, Decristoforo C, et al. MITIGATE-NeoBOMB1, a phase I/IIa study to evaluate safety, pharmacokinetics, and preliminary imaging of (68)Ga-NeoBOMB1, a gastrin-releasing peptide receptor antagonist, in GIST patients. J Nucl Med. 2020;61:1749–55.
55. Dalm SU, Bakker IL, de Blois E, et al. 68Ga/177Lu-NeoBOMB1, a novel radiolabeled GRPR antagonist for theranostic use in oncology. J Nucl Med. 2017;58:293–9.
56. Gourni E, Del Pozzo L, Kheirallah E, et al. Copper-64 labeled macrobicyclic sarcophagine coupled to a GRP receptor antagonist shows great promise for PET imaging of prostate cancer. Mol Pharm. 2015;12:2781–90.
57. Huynh TT, van Dam EM, Sreekumar S, et al. Copper-67-labeled bombesin peptide for targeted radionuclide therapy of prostate cancer. Pharmaceuticals (Basel). 2022;15(6):728. https://doi.org/10.3390/ph15060728
58. Rivera-Bravo B, Ramirez-Nava G, Mendoza-Figueroa MJ, et al. [(68)Ga]Ga-iPSMA-Lys(3)-bombesin: biokinetics, dosimetry and first patient PET/CT imaging. Nucl Med Biol. 2021;96-97:54–60.
59. Sartor O, Reid RH, Hoskin PJ, et al. Samarium-153-lexidronam complex for treatment of painful bone metastases in hormone-refractory prostate cancer. Urology. 2004;63:940–5.
60. Lawal IO, Mokoala KMG, Mahapane J, et al. A prospective intra-individual comparison of [(68)Ga]Ga-PSMA-11 PET/CT, [(68)Ga]Ga-NODAGA(ZOL) PET/CT, and [(99m)Tc]Tc-MDP bone scintigraphy for radionuclide imaging of prostate cancer skeletal metastases. Eur J Nucl Med Mol Imaging. 2021;48:134–42.
61. Fernandez R, Eppard E, Lehnert W, et al. Evaluation of safety and dosimetry of (177)Lu-DOTA-ZOL for therapy of bone metastases. J Nucl Med. 2021;62:1126–32.
62. Parker C, Nilsson S, Heinrich D, et al. Alpha emitter radium-223 and survival in metastatic prostate cancer. N Engl J Med. 2013;369:213–23.
63. Morris MJ, Loriot Y, Sweeney CJ, et al. Radium-223 in combination with docetaxel in patients with castration-resistant prostate cancer and bone metastases: a phase 1 dose escalation/randomised phase 2a trial. Eur J Cancer. 2019;114:107–16.
64. Geva R, Lopez J, Danson S, et al. Radium-223 in combination with paclitaxel in cancer patients with bone metastases: safety results from an open-label, multicenter phase Ib study. Eur J Nucl Med Mol Imaging. 2019;46:1092–101.
65. Smith M, Parker C, Saad F, et al. Addition of radium-223 to abiraterone acetate and prednisone or prednisolone in patients with castration-resistant prostate cancer and bone metastases (ERA 223): a randomised, double-blind, placebo-controlled, phase 3 trial. Lancet Oncol. 2019;20:408–19.
66. Ueno NT, Tahara RK, Fujii T, et al. Phase II study of Radium-223 dichloride combined with hormonal therapy for hormone receptor-positive, bone-dominant metastatic breast cancer. Cancer Med. 2020;9:1025–32.
67. Pryma DA, Chin BB, Noto RB, et al. Efficacy and safety of high-specific-activity (131)I-MIBG therapy in patients with advanced pheochromocytoma or paraganglioma. J Nucl Med. 2019;60:623–30.
68. Satapathy S, Mittal BR, Bhansali A. Peptide receptor radionuclide therapy in the management of advanced

pheochromocytoma and paraganglioma: a systematic review and meta-analysis. Clin Endocrinol. 2019;91: 718–27.
69. Yadav MP, Ballal S, Sahoo RK, Bal C. Efficacy and safety of (225)Ac-DOTATATE targeted alpha therapy in metastatic paragangliomas: a pilot study. Eur J Nucl Med Mol Imaging. 2022;49:1595–606.
70. Mastrangelo S, Tornesello A, Diociaiuti L, et al. Treatment of advanced neuroblastoma: feasibility and therapeutic potential of a novel approach combining 131-I-MIBG and multiple drug chemotherapy. Br J Cancer. 2001;84:460–4.
71. Kraal KC, Tytgat GA, van Eck-Smit BL, Kam B, Caron HN, van Noesel M. Upfront treatment of high-risk neuroblastoma with a combination of 131I-MIBG and topotecan. Pediatr Blood Cancer. 2015;62:1886–91.
72. Ferdinandus J, Costa PF, Kessler L, et al. Initial clinical experience with (90)Y-FAPI-46 radioligand therapy for advanced-stage solid tumors: a case series of 9 patients. J Nucl Med. 2022;63:727–34.
73. Baum RP, Schuchardt C, Singh A, et al. Feasibility, biodistribution, and preliminary dosimetry in peptide-targeted radionuclide therapy of diverse adenocarcinomas using (177)Lu-FAP-2286: first-in-humans results. J Nucl Med. 2022;63:415–23.
74. Liu XQ, Fourel L, Dalonneau F, et al. Biomaterial-enabled delivery of SDF-1alpha at the ventral side of breast cancer cells reveals a crosstalk between cell receptors to promote the invasive phenotype. Biomaterials. 2017;127:61–74.
75. Lapa C, Herrmann K, Schirbel A, et al. CXCR4-directed endoradiotherapy induces high response rates in extramedullary relapsed Multiple Myeloma. Theranostics. 2017;7:1589–97.
76. Habringer S, Lapa C, Herhaus P, et al. Dual targeting of acute leukemia and supporting niche by CXCR4-directed theranostics. Theranostics. 2018;8:369–83.
77. Lapa C, Hanscheid H, Kircher M, et al. Feasibility of CXCR4-directed radioligand therapy in advanced diffuse large B-cell lymphoma. J Nucl Med. 2019;60:60–4.
78. Nautiyal A, Jha AK, Mithun S, et al. Analysis of absorbed dose in radioimmunotherapy with 177Lu-trastuzumab using two different imaging scenarios: a pilot study. Nucl Med Commun. 2021;42:1382–95.
79. Quigley NG, Steiger K, Hoberuck S, et al. PET/CT imaging of head-and-neck and pancreatic cancer in humans by targeting the "Cancer Integrin" alphavbeta6 with Ga-68-Trivehexin. Eur J Nucl Med Mol Imaging. 2022;49:1136–47.